Antibacterial Graphene-Based Hydroxyapatite/Chitosan Coating with Gentamicin for Potential Applications in Bone Tissue Engineering

Milena Stevanović[1], Marija Djošić[2], Ana Janković[1], Vesna Kojić[3], Maja Vukašinović-Sekulić[1], Jovica Stojanović[2], Jadranka Odović[4], Milkica Crevar Sakač[4], Kyong Yop Rhee[5] **, Vesna Mišković-Stanković[1,5] *

[1] *Faculty of Technology and Metallurgy, University of Belgrade, Karnegijeva 4, 11000 Belgrade, Serbia*

[2] *Institute for Technology of Nuclear and Other Mineral Raw Materials (ITNMS), Bulevar Franš d'Eperea 86, Belgrade, Serbia*

[3] *Oncology Institute of Vojvodina, Faculty of Medicine, University of Novi Sad, Put Dr Goldmana 4, 21204 Sremska Kamenica, Serbia*

[4] *Faculty of Pharmacy, University of Belgrade, 450 Vojvode Stepe Street, 11000 Belgrade, Serbia*

[5] *Department of Mechanical Engineering, Kyung Hee University, Yongin 449-701 South Korea*

*Corresponding author. Tel: + 381 11 3303 687; fax: + 381 11 3370 387. E-mail: vesna@tmf.bg.ac.rs

**Co-corresponding author. Fax: +82 31 202 6693. E-mail address: rheeky@khu.ac.kr (K.Y. Rhee)

This article has been accepted for publication and undergone full peer review but has not been through the copyediting, typesetting, pagination and proofreading process which may lead to differences between this version and the Version of Record. Please cite this article as doi: 10.1002/jbm.a.36974

Abstract

Electrophoretic deposition process (EPD) was successfully used for obtaining graphene (Gr) - reinforced composite coating based on hydroxyapatite (HAP), chitosan (CS) and antibiotic gentamicin (Gent), from aqueous suspension. The deposition process was performed as a single step process at a constant voltage (5 V, deposition time 12 min) on pure titanium foils. The influence of graphene was examined through detailed physico-chemical and biological characterization. Fourier transform infrared spectroscopy, field emission scanning electron microscopy, thermogravimetric analysis, X-ray diffraction, Raman and X-ray photoelectron analyses confirmed the formation of composite HAP/CS/Gr and HAP/CS/Gr/Gent coatings on Ti. Obtained coatings had porous, uniform, fracture-free surfaces, suggesting strong interfacial interaction between HAP, CS and Gr. Large specific area of graphene enabled strong bonding with chitosan, acting as nanofiller throughout the polymer matrix. Gentamicin addition strongly improved the antibacterial activity of HAP/CS/Gr/Gent coating that was confirmed by antibacterial activity kinetics in suspension and agar diffusion testing, while results indicated more pronounced antibacterial effect against *Staphylococcus aureus* (bactericidal, viable cells number reduction >3 logarithmic units) compared to *Escherichia coli* (bacteriostatic, <3 logarithmic units). MTT assay indicated low cytotoxicity (75 % cell viability) against MRC-5 and L929 (70 % cell viability) tested cell lines, indicating good biocompatibility of HAP/CS/Gr/Gent coating. Therefore, electrodeposited HAP/CS/Gr/Gent coating on Ti can be considered as a prospective material for bone tissue engineering as a hard tissue implant.

Keywords: Electrophoretic deposition; Antibacterial activity; Cytotoxicity; Graphene; Gentamicin.

1. Introduction

Titanium and its alloys are preferred biomaterials for hip, knee and joint replacements. Pure Ti is considered a reliable implant material that is inert in the body environment with a long-lasting feature.[1,2] Although it possesses a lot of qualities, pure Ti cannot sufficiently induce osseointegration process causing ineffective bone ingrowths. However, the biocompatibility and bioactivity of Ti can be significantly improved by modifying its surface by various processes. For developing biocompatible composite films on the Ti surface, electrophoretic deposition process (EPD) is considered a favorable technique that allows formation of diverse composite materials.[3,4]

An interesting choice for bone tissue regeneration coating material is hydroxyapatite (HAP), due to its biocompatibility and similarity with bone tissue.[5] HAP is a bioactive ceramic material, characterized by high biocompatibility and ability to form a direct chemical bond with bone tissue.[6] However, due to its brittleness and poor adhesion properties it is necessary to combine HAP with an adequate polymer to serve as a binder. The prospective solution represents the combination of biopolymer matrix and bioceramics, e.g. hydroxyapatite-based composite coatings with natural or synthetic polymers.[7] The most commonly used natural polymers are collagen,[8] gelatin,[9] alginate[10] and chitosan.[9,11,12] Synthetic polymers that are most often used in bone tissue engineering are poly(lactide-co-glycolide) (PLGA),[13] polycaprolactone (PCL),[14] poly(vinyl alcohol) (PVA),[11] poly(glycolic acid) (PGA),[15] poly(lactic acid) (PLA).[16,17] Chitosan (CS) is intensively investigated in the field of tissue engineering due to its unique properties, such as biodegradability, biocompatibility, adhesiveness and intrinsic antibacterial properties.[18,19] It is very important to point out that chitosan can mimic the structure of glycosaminoglycans in the bone extracellular matrix, contributing to the sponginess of the developed bone.[20,21] Hydrophilic surface of CS improves cell adhesion, differentiation and proliferation, minimizing, at the same time, the body response upon implantation.[22] In combination with HAP, chitosan contributes to improved mechanical, adhesion and antibacterial coating

properties, which is of particular importance for further application.[23] Also, the possibility of applying bone tissue composite coatings as a carrier of anti-infection drugs at the implantation site, as well as growth factors that stimulate the osteoblasts activity is the subject of investigation.[24]

Considering HAP brittleness, as well as low fracture toughness and poor tensile strength, graphene (Gr) inclusion in composite structures could improve mechanical, thermal and electrical properties of the composites, while good biocompatibility makes it a promising biomaterial.[25,26] When used as reinforcement filler in composites with HAP and polymers, Gr could induce increased bone formation ability, increased specific area, smaller grain size and could elevate the negative surface charge attracting more calcium and forming bone-like layer,[27] as well as good cytocompatibility.[28] Nowadays, there is a growing need for development of antibacterial drug-eluting coatings which will prevent biofilm occurrence and treat implant-associated infections.[29] This type of coating should ensure the long-term drug action through controlled release of the drug at the implantation site overcoming the problems associated with bone infection occurrence. Locally administrated antibiotic has less susceptibility to promote antibiotic resistance achieving at the same time long-term antibiotic release with lower applied antibiotic doses.[30] Antibiotic-loaded composites obtained by EPD technique have gained much attention in recent studies when vancomycin,[31] tobramycin,[32] ciprofloxacin,[4] ampicillin,[33] tetracycline,[34] levofloxacin,[35] ibuprofen[34] and gentamicin[18] have been successfully included in composites aimed for controlled drug delivery. Depending on the nature of the infection or the inflammatory process, different types of antibiotics can be selected for treatment. One of the antibiotics that are often used to treat post-surgery osteomyelitis is gentamicin. Gentamicin, a water-soluble aminoglycoside antibiotic, is known to have very potent antibacterial activity for the treatment of wide range of infections, caused by both Gram-negative and Gram-positive bacteria.[18,36,37]

The principal objective of the research was to obtain improved Gr-reinforced antibacterial composite HAP/CS coatings, with and without gentamicin, on Ti substrate using electrophoretic deposition technique from aqueous suspension since antibiotic-loaded coatings are intended for medical use. To our knowledge, based on previously published literature, this is the first time that the single step deposition from four-component HAP/CS/Gr/Gent aqueous suspension, with no additional treatment, was performed.

2. Experimental

2.1. Materials

The following materials were all purchased from Sigma-Aldrich and used to assemble composite coatings on Ti surface: powders of HAP (particles < 200 nm), chitosan (medium molecular weight (190−310) kDa, degree of deacetylation 75−85 %), and gentamicin sulfate solution (50 mg/mL in dH_2O). Pure graphene nanopowder (99.2 %) with average graphene nanoflakes thickness of 12 nm was purchased from Graphene Supermarket, USA. Before EPD, titanium plates (15 × 10 × 0.25 mm, 99.7 %) were mechanically polished and ultrasonicated (15 min in acetone). Methanol, o-phtalaldehyde, 2- mercaptoethanol, boric acid, sodium hydroxide, and 2-propanol (all purchased from Merck, Germany) were used for gentamicin derivatization procedure. The mobile phase consisted of sodium octanesulfonate and glacial acetic acid (Merck, Germany).

2.2. Electrophoretic deposition

Aqueous suspensions containing 1 wt % HAP nanopowder, 0.05 wt % chitosan, 0.01 wt % graphene and 0.1 wt % gentamicin sulfate were used for EPD process in order to obtain HAP/CS/Gr and HAP/CS/Gr/Gent composite coatings, according to our previously published procedure.[18] Suspensions pH value was adjusted to 4.4. Cataphoretic deposition was performed on pure Ti plate, serving as a working electrode (cathode), at constant voltage of 5 V for deposition time of 12 min. Two parallel

platinum plates were used as counter electrodes (anodes). After deposition was performed, coatings were dried at room temperature for 24 h, while the thicknesses were 3.0±1.5 μm and 3.2±0.9 μm for HAP/CS/Gr and for HAP/CS/Gr/Gent coating, respectively.

2.3. Characterization

The instrument LEO SUPRA 55 (Carl Zeiss AG, Germany) operating at 10 kV voltage acceleration was used for field-emission scanning electron microscopy (FE-SEM) equipped with In-Lens detector and combined SE-BSE mode was used. Fourier transform infrared spectroscopic studies (FTIR) were carried out on a machine Nicolet IS-50 (Thermo Fisher Scientific, USA) in ATR mode in the range of 400−4000 cm^{-1} (4 cm^{-1} spectral resolution). X-ray photoelectron spectroscopy (XPS) spectra were recorded using a K Alpha System photoelectron spectroscope (Thermo Electron, USA), with monochromatic Al Kα X-ray (1486.6 eV) excitation source. The adventitious carbon peak maximum in the C 1s spectra was set as 284.8 eV. OriginPro 9 software was used for peak fitting, with previous Shirley-type background correction. Raman analysis was carried out by a Renishaw Invia (Renishaw plc, UK) Raman spectrophotometer (514-nm argon laser) with 10 % intensity of the total power and in the spectral range from 3500 to 100 cm^{-1}. Thermogravimetric analysis (TGA) was performed by TGA Q5000 IR/SDT Q600 instrument (TA Instruments, USA), operating in 30-1000 °C range at a heating rate of 20 °C/min in inert atmosphere (N_2, 50 mL/min). X-ray diffraction analysis (XRD) was performed by powder diffractometer Philips PW 1710 (Philips, Netherland) with Ni-filtered Cu Kα radiation (λ = 1.5418 Å). Diffraction intensity was recorded at room temperature, between 10−70°, 0.05° step. For phase analysis, PowderCell software was used. Gentamicin content was estimated by HPLC chromatography using Dionex UltiMate 3000 HPLC system (Thermo Fisher Scientific, USA) with Chromolith RP-18 column (Merck, Germany). Gentamicin in the solution was derivatized prior to HPLC (ultraviolet (UV) detector) loading, as described in our previously published paper.[18] Main gentamicin components were detected by UV detector at 330 nm.

2.4. Biological measurements

2.4.1. Antibacterial activity and cytotoxicity

HAP/CS/Gr and HAP/CS/Gr/Gent coatings presumed antibacterial activity was evaluated against *Staphylococcus aureus* TL (culture collection-FTM, University of Belgrade, Serbia) and *Escherichia coli* ATCC 25922, by agar diffusion method and quantitatively by monitoring changes in the viable number of bacterial cells in suspension. Both antibacterial assays were performed according to our previously published paper.[18]

Cytotoxicity of HAP/CS/Gr and HAP/CS/Gr/Gent coatings against mice origin fibroblast cell line L929 (ATCC CRL-6364) and MRC-5 cell line (human origin fibroblasts) was determined by MTT test according to the FDA Biological Evaluation Guidance - International Standard ISO 10993-1[38] and experimental procedure reported in our previously published work.[18]

3. Results

In general, the main advantages of EPD technique are: (a) the ability to produce coatings on metal surfaces of complex shapes, (b) the cleanliness of the process without the use of potentially toxic chemicals, thus producing biocompatible materials that are safe for medical use, and (c) coating fabrication at room temperature, which is of particular importance for drug and biologically active molecules processing. Since the gentamicin is water-soluble, deposition of HAP/CS/Gr/Gent coating on titanium surface was performed from aqueous solution in a single step, i.e co-precipitation from a four-component aqueous suspension has occurred. This is a remarkable advantage over the data available so far in the literature relating to bioactive coatings deposited in several steps.[39–41]

Due to the electrolysis of water, hydrogen and oxygen evolution occurs on the cathode and anode, respectively (Eqs. 1 and 3).

cathode: $2H_2O + 2e^- \rightarrow H_2 + 2OH^-$ (1)

$CS–NH_3^+ + OH^- \rightarrow CS–NH_2 + H_2O$ (2)

anode: $2H_2O \rightarrow 4H^+ + O_2 + 4e^-$ (3)

Chitosan is soluble in aqueous solutions, at lower pH values (slightly acidified environment), due to the protonation of amine groups, e.g. CS-NH_3^+.[3,18,42] Protonated amine groups of the CS molecule in acidic media facilitate electrostatic interactions between individual CS chains, increasing the overall suspension stability. The deposition of insoluble chitosan CS-NH_2 coating occurred due to CS-NH_3^+ and OH^- ions interaction on the cathode (Eq. 2) since OH^- ions are being formed as a result of electrochemical water decomposition (Eq. 1). When HAP inorganic particles were added in slightly acidic solution, the protonation of HAP surface occurred. Special attention should be paid on to the addition of graphene, aimed to serve as reinforcement filler. Gr is known to form strong bond with chitosan matrix, as a consequence of its characteristic surface architecture, i.e. great number of p electrons in sp^2 hybrid orbitals inducing the negative charge on the Gr sheet surface. Negatively charged surface of Gr could interact with protonated amino groups of chitosan, forming a stable suspension for the coating deposition process.[43] On the other hand, Van der Waals interaction between graphene sheets and HAP, through the calcium ions, occurred as well.[44,45] Therefore, all particles (CS, Gr and HAP) interact with each other, making well-dispersed suspension suitable for composite coating deposition. For HAP/CS/Gr coating loaded with gentamicin, positively charged Gent (due to the protonation of amino and hydroxyl groups[41]) migrated toward the cathode and formed a four-component coating along with HAP, CS and Gr.

3.1. FTIR analysis

The characteristic FTIR spectral bands for HAP/CS/Gr and HAP/CS/Gr/Gent coatings in the region from 400 to 4000 cm^{-1} are represented in Figs. 1a and b, respectively. Specific spectral region deconvolutions are given for HAP/CS/Gr coating (Figs. 1c and d). The influence of antibiotic addition

on FTIR spectra was represented for HAP/CS/Gr and HAP/CS/Gr/Gent coatings (Figs. 1e and f, respectively).

Spectral carbonate bands for HAP/CS/Gr composite coating were observed in the regions from 800 to 900 cm^{-1} and from 1350 to 1600 cm^{-1} (Fig. 1a).[46] Carbonate ions can substitute hydroxyl and/or phosphate groups, leading to formation of carbonate substituted HAP. When the replacement of OH^- groups by CO_3^{2-} groups occurs, the change in HAP structure is known as A-type substituted HAP. When PO_4^{3-} groups are substituted by CO_3^{2-} groups, then such substitution is denoted as B-type hydroxyapatite.[46] In FTIR spectra for HAP/CS/Gr composite coating (Fig. 1a), observed carbonate band at 878 cm^{-1} represents the vibration mode of O–C–O group.[18,46] With the aim to determine the type of carbonate substitution in HAP, deconvolution of carbonate peak in the region 800-900 cm^{-1} (Fig. 1c) and 1350-1600 cm^{-1} (Fig. 1d) was performed. The deconvolution of carbonate band at 878 cm^{-1} revealed three different peaks (Fig. 1c). A peak at 879 cm^{-1} can be assigned to the A-type carbonate substitution, peak at 872 cm^{-1} suggested the presence of B-type substitution, while the peak at 865 cm^{-1} represented the non-apatitic carbonate.[47] The deconvolution of FTIR peaks in the region from 1350 to 1600 cm^{-1} (Fig. 1d) confirmed the presence of A- and B-type of substitution in HAP, as well. Bands at 1421 and 1470 cm^{-1}, as well as a doublet at 1407 and 1441 cm^{-1}, can be assigned to B-type,[48] while the presence of a band at 1528 cm^{-1},[46] suggested the A-type substitution in HAP (Fig.1d). A band at 1456 cm^{-1} can be assigned to the both A and B-type of carbonate substituted HAP.[47] Based on the positions of all carbonate bands, it could be concluded that "AB-type" substitution occurred in HAP/CS/Gr. The carbonate substitution in HAP structure is advantageous regarding bioactivity and similarity to the natural bone.[47] Two distinctive bands at 1654 cm^{-1} (amide I band) and 1546 cm^{-1} (amide II band) for HAP/CS/Gr coating (Fig. 1e) were assigned to the C=O stretching vibration of –NHCO– group and the N–H bending in $–NH_2$ group of CS, respectively.[18,49] The chitosan presence in HAP/CS/Gr coating was also verified by bands at 2857 cm^{-1} and 2926 cm^{-1} (Fig. 1a), originating from

C-H stretching in the CS structure.[49,50] At 1388 cm^{-1} (Fig. 1d) the band for CH_3 symmetrical deformation in chitosan structure can be distinguish.[51] The bands at 473, 563, 600, 952, 1020 and 1085 cm^{-1} undoubtedly confirmed the hydroxyapatite presence in the HAP/CS/Gr composite coating. All these bands were ascribed to the different vibration modes of PO_4^{3-} group.[18]

Band at 1560 cm^{-1} (Fig. 1e) can be assigned to the skeletal vibration of Gr, confirming the successful incorporation of graphene in HAP/CS/Gr composite coating.[43,52] Inset in Figure 1a highlights the region from 3000 to 3600 cm^{-1}, where prominent peak at 3570 cm^{-1} was observed, corresponding to -OH stretching from HAP structure.[53] A wide band at around 3279 cm^{-1} (for HAP/CS/Gr) can be attributed to the valence vibrations of hydroxyl groups, sensitive to hydrogen bonding.[49] Therefore, it can be assumed that hydrogen bonding between hydroxyl groups of HAP and hydroxyl and amino groups of CS occurred. In Fig. 1b FTIR spectrum for HAP/CS/Gr/Gent coating is represented. Generally, characteristic bands, corresponding to HAP, chitosan and graphene can be observed for HAP/CS/Gr/Gent coatings, as it was reported for HAP/CS/Gr coating (Fig. 1a). After gentamicin incorporation in HAP/CS/Gr/Gent coating, a new band at 1640 cm^{-1} appeared (Fig. 1f). This band can be assigned to the N-H bending vibration of primary aromatic amines,[54] confirming gentamicin presence in composite coatings. Additional confirmation of the gentamicin interaction with apatite and chitosan can be obtained in the FTIR spectra through the shift of the characteristic chitosan bands to the lower wavenumbers. The slight shift from 3279 cm^{-1} (for HAP/CS/Gr, Inset in Fig. 1a) to 3261 cm^{-1} (HAP/CS/Gr/Gent, Inset in Fig. 1b)) was noticed after gentamicin introduction. These bands were attributed to the valence vibrations of hydroxyl groups, sensitive to hydrogen bonding.[49] Therefore it can be assumed that hydrogen bonding between hydroxyl groups of HAP and amino and hydroxyl groups of CS with newly introduced gentamicin hydroxyl and amino groups occurred.

3.2. XRD analysis

XRD analyses of HAP/CS/Gr and HAP/CS/Gr/Gent coatings (Figs. 2a and b, respectively), revealed presence of HAP (JCPDS 09-0432) and Ti (JCPDS 89-2762), that originated from the substrate. CS, Gr and Gent peaks cannot be detected, probably due to the small amount of these components in the composite coatings; their peaks are overlapped by much stronger HAP diffraction maxima. In both composite coatings (Figs. 2a and b), diffraction maxima are broadened, suggesting that HAP crystallites have fine crystallite size. XRD diffractograms exhibited higher intensities of diffraction maxima for HAP/CS/Gr compared to the HAP/CS/Gr/Gent coating, indicating that more HAP crystals were formed in the case of HAP/CS/Gr. Using the HAP characteristic crystal planes ((002), (211), (112) and (300)), *d*-spacing values (Table 1), unit cell volume (*V*) unit cell parameters (*a* and *c*) and crystallite domain size (Table 2) were calculated. As a consequence of gentamicin incorporation, a decrease in the *d*-spacing values for HAP/CS/Gr/Gent coating with respect to the HAP/CS/Gr coating can be observed (Table 1). Gentamicin as aminoglycoside antibiotic has numerous amino and hydroxyl moieties, enabling the interaction with the –OH groups of HAP through hydrogen bonding or electrostatic interactions.[4] Additionally, bonding can occur through the mutual interaction of hydroxyl and amino groups from CS and Gent. All of these interactions are accompanied by the intermolecular bonding, causing the contracting in the chitosan matrix and consequently decreasing HAP *d*-spacing value.[55] As a consequence, the unit cell parameters (*a* and *c*) and the unit cell volume (*V*), as well as the crystallite domain size have smaller values for HAP/CS/Gr/Gent coating than for the HAP/CS/Gr coating (Table 2). Crystallite domain size depends on crystallization rate and the rate of crystal growth. During the coating drying process, sulfate ions (from the gentamicin sulfate) influence the formation of a large number of nucleation sites. At the same time, as gentamicin is a bulky molecule, there is also a possibility that it prevents further crystal growth. Both of these effects lead to finer crystallite structure and smaller size in the case of HAP/CS/Gr/Gent, which contributes to

better osseointegration due to bone-like apatite formation.[56,57] Namely, owing to their large surface-to-volume ratio HAP nanoparticles are considered to improve the *in vitro* bone-like apatite formation, by increasing the specific area of biomaterial.[58,59] Moreover, it was shown that a larger contact area enhanced the adhesive protein adsorption and thus contributed to the interactions between cells and biomaterial surfaces.[4,60] The higher amount of adsorbed proteins was in correlation with a larger specific area, justifying the statement of improved bioactivity when smaller particles are used.[61]

3.3. XPS analysis

The deconvoluted high resolution XPS spectra of C 1s, O 1s, and N 1s of HAP/CS/Gr and HAP/CS/Gr/Gent coatings are depicted in Fig. 3. C 1s peak was fitted into five different modes (Fig. 3a) which were assigned to C–H/C–C (284.6 eV), C–O/C–N (285.5 eV), O–C–O (286.9 eV), O-C═N (288.65 eV) and C═O (290.2 eV) originating from Gr,[62] and acetyl and amide groups characteristic for CS.[63] Similar BE at 284.8, 285.8, 287.2, 288.8, and 290.3 eV, for C 1s peaks were also found for HAP/CS/Gr/Gent (Fig. 3b) and were ascribed to C–H/C–C, C–O/C-N, O–C–O, O–C═N, and C═O, respectively. Characteristic peaks for gentamicin at 287.2 eV (O–C–O) and 288.8 eV, (O–C═N) originating from acetal bonds and methylamino groups from gentamicin, overlapped with acetal and amide groups from CS[64,65] so similar peaks were obtained for both coatings. The high-resolution O 1s peak was fitted into three different modes (Fig. 3c and d). Peaks at 531.4 and 531.7 eV for HAP/CS/Gr and HAP/CS/Gr/Gent, respectively could be assigned to the PO_4^{3-} groups of HAP, while peaks at 532.7 eV for both samples could represent the contribution from hydroxyl groups from HAP, CS and Gent. The peaks at 533.6 for HAP/CS/Gr and 533.8 eV for HAP/CS/Gr/Gent could be assigned to the C═O interactions, originating from chitosan and gentamicin.[18] Figs 3e and 3f represent the deconvolution of high resolution N 1s spectra for HAP/CS/Gr and HAP/CS/Gr/Gent. The peaks at 400.2 and 400.5 eV, for HAP/CS/Gr and HAP/CS/Gr/Gent, respectively were assigned to $C–NH_2$ interactions (free amines),[66] while peaks at 401.7 eV for both spectra could be assigned to the $C–NH_3^+$

interactions (protonated amines).[18,64] Since gentamicin sulfate solution was used, XPS spectrum of HAP/CS/Gr/Gent composite displayed the S 2p peak, clearly confirming the gentamicin incorporation. S 2p peak (data not shown) was fitted with peak component at 170 eV.[18] Elemental composition, calculated from XPS (Table 3) confirmed the gentamicin incorporation through the sulfur content in the HAP/CS/Gr/Gent coating (0.7 at %). The calculated values of Ca/P ratio of 1.26 and 1.27 for HAP/CS/Gr and HAP/CS/Gr/Gent coatings, respectively, confirmed the FTIR conclusion on calcium-deficient HAP. It is known that bioactivity and osteoinductivity are improved in the case of substituted HAP compared to the HAP that retains stoichiometric ratio.[67,68]

3.4. FE-SEM

Fig. 4 represents the morphology of HAP/CS/Gr (Figs. 4a and b) and HAP/CS/Gr/Gent (Figs. 4c and d) coatings at different magnifications. By examining the surface of the HAP/CS/Gr coating, a large number of spherical particles of different sizes is evident (Fig. 4a), corresponding to HAP finely and uniformly dispersed within a polymer/graphene matrix. At lower magnification (Figs. 4a and c), the chitosan can be observed as a wax-like matrix for both coatings. The surface of HAP/CS/Gr/Gent coating (Fig. 4c) exhibited few cracks, probably formed during the air drying process due to higher water content in HAP/CS/Gr/Gent coating (according to TG analysis, presented below (Section 3.6.) and polymer matrix shrinkage during drying process. Due to similar morphology of HAP/CS/Gr and HAP/CS/Gr/Gent coatings, the incorporation of gentamicin did not significantly affect the surfaces on the micro level, as can be clearly seen from Fig 4c and d. At higher magnification, the surface of HAP/CS/Gr (Fig. 4b) consisted of HAP spherical particles which are mostly agglomerated and covered with small HAP particles. Agglomeration of particles could occur due to interface interaction between HAP and polymer matrix and was attributed to the high specific surface energy of HAP particles.[55] Even at higher magnification, the surface of both coatings (Figs. 4b and d) seems porous and homogeneous. This well-dispersed network is reinforced by Gr, known to act as a “bonding”

material, making bridges through polymer matrix and preventing the crack formation in the coatings.[69]

3.5. Raman spectroscopy

Figs. 5a and b represent the Raman spectra of HAP/CS/Gr and HAP/CS/Gr/Gent coatings, respectively. The first difference was spotted in the wavenumber and the intensity of the band corresponding to γ_1 stretching vibrations of PO_4^{3-} group which was decreased in HAP/CS/Gr/Gent coating (920 cm^{-1}) with respect to HAP/CS/Gr coating (959 cm^{-1}). Gentamicin introduction caused a change in the vibrational mode of PO_4^{3-} through establishing chemical bonds between hydroxyl groups of HAP with OH^- groups from CS and gentamicin. Further, the band at 1566 cm^{-1}, assigned to the G-band characteristic for Gr overlapping with in-plane bending vibrations of $–NH_2$ bonds from CS[70,71] was evident in the HAP/CS/Gr spectrum, whereas for HAP/CS/Gr/Gent this band was not observed due to the interactions between amino groups of CS and Gent. However, bands at 1358 cm^{-1} and 1372 cm^{-1} for HAP/CS/Gr and HAP/CS/Gr/Gent, respectively, originating from D-band (associated with the disorder in Gr structure), indicated the graphene incorporation. Moreover, characteristic 2D-band for Gr presence was noticed at 2704 cm^{-1} for HAP/CS/Gr and at 2728 cm^{-1} for HAP/CS/Gr/Gent.[71] Spectral bands found at 2936 cm^{-1} and 2912 cm^{-1} in the case of HAP/CS/Gr and HAP/CS/Gr/Gent, respectively, were assigned to the symmetric stretching of the C-H bond from the $–CH_2$ group in the CS. After introduction of gentamicin, the band at 2912 cm^{-1} became more pronounced in comparison to the peak at 2936 cm^{-1} due to the change in vibration modes of –CH and $–CH_2$ groups after gentamicin introduction.[49]

3.6. Thermal stability

TG/DTG analysis was performed to investigate the thermal stability of HAP/CS/Gr and HAP/CS/Gr/Gent composite coatings (Figs. 6a and b, respectively) and to examine the influence of gentamicin on the thermal properties of HAP/CS/Gr/Gent coating.

HAP/CS/Gr and HAP/CS/Gr/Gent coatings expressed gradual weight loss through several steps. Gentamicin addition caused significant increase in the initial mass loss (2.6 wt % (16-118 °C) for HAP/CS/Gr compared to 6.5 wt % (18-158 °C) for HAP/CS/Gr/Gent), ascribed to the water desorption, due to reduced crystallite domain size, i.e. larger specific surface area of HAP/CS/Gr/Gent coating compared to HAP/CS/Gr coating, as it was shown by XRD results. Next mass loss stage was assigned to the crystalline water release and the beginning of HAP dehydroxylation[43] in the temperature interval from 166 to 212 °C (0.6 wt % mass loss) for HAP/CS/Gr and 117-238 °C (1.2 wt % mass loss) for HAP/CS/Gr/Gent coating. In the third mass loss stage (240-345°C (1.4 wt %) for HAP/CS/Gr and 213-365 °C (2.4 wt %) for HAP/CS/Gr/Gent), thermal decomposition of chitosan,[72] along with gentamicin decomposition took place.[73] Moreover, DTG analysis pointed to the prominent peak at 294 °C (ascribed as CS degradation) for HAP/CS/Gent coating (Fig 6a) which was shifted to 305 °C for HAP/CS/Gr/Gent coating (Fig 6b). Bearing in mind that HAP in both coatings is carbonate substituted, as confirmed by the FTIR analysis, next mass losses of 1.2 wt % (345-433 °C) for HAP/CS/Gr and 0.7 wt % (364-425 °C) for HAP/CS/Gr/Gent coating were assigned to the loss of carbonate ions as CO_2 as well as to the further degradation of chitosan (for HAP/CS/Gr coating) and chitosan and gentamicin (for HAP/CS/Gr/Gent coating).[41,74] In the next mass loss stage with 0.5 wt % mass loss (433-509 °C) for HAP/CS/Gr and 1.4 wt % mass loss (425-580 °C) for HAP/CS/Gr/Gent coatings two maxima on the DTG curve (Fig 6a and b) at 443 °C for HAP/CS/Gr coating and at 450 °C for HAP/CS/Gr/Gent coating were observed. These two peaks can be attributed to the decomposition of Gr in composites,[75,76] along with loss of carbonate ions from HAP structure, to the decomposition of the remaining components from CS, as well as to the loss of Gent residual functional groups.[74,77–79] In the last stage with 1.8 wt % mass loss (514-685 °C) for HAP/CS/Gr coating and 0.8 wt % mass loss (582-662 °C) for HAP/CS/Gr/Gent coating, decarbonation and dehydroxylation processes of HAP took place.[78] Greater total mass loss was observed for

HAP/CS/Gr/Gent coating (14.8 wt %) compared to HAP/CS/Gr coating (10.5 wt %) indicating its lower thermal stability.

3.7. Gentamicin content

The overall antibiotic content (measured in triplicate) was determined using the HPLC-UV method after the derivatization procedure. The three most dominant gentamicin components are C1, C1a, and C2 with minor differences in their structure and similar antibiotic activity[80] for which the obtained retention times were approximately 3.3, 6.4, and 9.8 min. The average amount of gentamicin per 1 cm^2 of HAP/CS/Gr/Gent coating was 8.2 ± 0.1 μg. Compared to previously published results[18] for HAP/CS/Gent coating of 7.3 ± 0.1 μg per cm^2, this increase of more than 10 wt % is substantial and clearly the result of graphene presence in the coating, not surprisingly as Gr represents a powerful nano-platform for antibiotic gentamicin loading.[79]

3.8. Antibacterial activity and cytotoxicity evaluation

Gentamicin, like most aminoglycosides, irreversibly binds to specific subunit proteins (30S) and 16S rRNA in the bacterial cell. This binding causes t-RNA misreading that prevents the synthesis of vital proteins. More precisely, gentamicin binds to four 16S rRNA nucleotides and a protein S12 amino acid, causing interference in the decoding site close to the nucleotide 1400 in 16S rRNA of 30S subunit. This region interacts with the wobble base in the anticodon of tRNA, leading to initiation complex interference, polysomes breakup into nonfunctional monosomes, as well as a misreading of mRNA that causes incorrect amino acids to be inserted into the polypeptide.[81–83]

The antibacterial efficacy of HAP/CS/Gr/Gent (1 mg/mL gentamicin) and HAP/CS/Gr coatings was investigated using the agar diffusion method and the results are presented in Fig. 7. Pure gentamicin solution in the presence of *S. aureus* TL and *E. coli* ATCC 25922 was used as a control (D =10 mm), causing clear, wide inhibition zone (31 mm in diameter, Fig. 7a) in the *S. aureus* TL presence. However, *E. coli* ATCC 25922 responded with wide inhibition zone consisting of brighter

(D=24 mm) and darker (D=30 mm) inhibition regions indicating maximum and moderate bacterial sensitivity, respectively (Fig. 7b). Neither of the bacteria was sensitive to HAP/CS/Gr coating as indicated by inhibition zone absence (Fig. 7a and b, sample 1). Contrary to HAP/CS/Gr, HAP/CS/Gr/Gent coating exhibited wide inhibition zone (36 × 27 mm) (Fig. 7a, sample 2) against *S. aureus* TL and 2 sensitivity zones against *E. coli* (Fig. 7b, sample 2): a brighter (24 × 21 mm) and a darker one (28 × 25 mm). The propagation of the inhibition zones for HAP/CS/Gr/Gent is an indication that even low concentration (1 mg/mL) of added gentamicin provided for efficient antibacterial activity. However, more pronounced antibacterial effect of the HAP/CS/Gr/Gent in the presence of *S. aureus*, rather than *E. coli*, represents an additional selectivity feature of the material.

Figs. 8a and b depict the effect of HAP/CS/Gr and HAP/CS/Gr/Gent coating against *S. aureus* TL and *E. coli* ATCC 25922 in PB medium, respectively, using test in suspension, simulating static *in vitro* conditions. Even though, CS and Gr and Gr-related species antimicrobial effect is well documented in literature,[84,85] expected synergistic effect of composite HAP/CS/Gr could not be verified. In Figs. 8a and b, bacteria incubated without any coated sample (control) and bacteria in the presence of HAP/CS/Gr follow the same growth pattern i.e. numbers of viable cells are the same within the margin of error. Immediately after inoculation HAP/CS/Gr/Gent coating expressed strong bactericidal effect against *S. aureus*, reducing the initial bacteria count by 2 logarithmic units. However, in the first hour, drug release seems to be delayed, indicating the strong hydrogen bonding reinforced through non-specific interaction of gentamicin to chitosan and graphene. Diminishing of *S. aureus* bacterial growth occurred within 3 h of exposure (Fig. 8a). Based on the results of HAP/CS/Gr/Gent composite coating against *S. aureus*, the effect is highly bactericidal.[86] Retained antibacterial effect of HAP/CS/Gr/Gent coating was clearly seen against *E. coli* (Fig. 8b). In the initial period after inoculation the release of the drug hardly affected the bacteria i.e. their sensitivity towards antibiotic was low. For the duration of the experiment (24 h post incubation) substantial decline of surviving

E. coli cells was observed. Comparing the effects of composite HAP/CS/Gr and HAP/CS/Gr/Gent coatings and based on the kinetics testing against *E. coli*, since the reduction in bacterial cells was less than 3 logarithmic units, HAP/CS/Gr/Gent coating was classified as bacteriostatic.[86]

MTT test was employed for the *in vitro* cytotoxicity evaluation of the targeted two cell lines, MRC-5 (human fibroblasts) and L929 (mice fibroblasts). HAP/CS/Gr and HAP/CS/Gr/Gent were compared using the standard MTT assay for the estimation of the number of viable cells that convert water-soluble yellow MTT dye into an insoluble purple formazan. Spectrophotometrically determined formazan amount at 540/690 nm is directly proportional to the number of live cells, estimating the extent of cytotoxicity. The MTT assay results are represented in Fig. 9, comparing the cell viability in the presence of HAP/CS/Gr and HAP/CS/Gr/Gent with control (blank containing cells only). According to one of the material cytotoxicity scales,[87] there is no evidence of cytotoxicity for HAP/CS/Gr for both tested cell lines (viability > 90 %) while in the case of HAP/CS/Gr/Gent slight cytotoxicity was observed (60−90% viability). The L929 cell line exhibited slightly decreased viability in the presence of both samples, as compared with MRC-5 cell line which could be explained by elevated L929 cell sensitivity.

4. Discussion

EPD was successfully used for producing biocomposite HAP/CS/Gr and HAP/CS/Gr/Gent coatings from aqueous suspensions on the Ti substrate. The key feature of gentamicin transfer and incorporation was quantified by HPLC-UV, yielding the calculated value of 8.2 ± 0.1 μg per 1 cm^2 for HAP/CS/Gr/Gent. Despite low total concentration of antibiotic in the composite HAP/CS/Gr/Gent coating, antibacterial assays confirmed the efficiency of this concentration against *E. coli* and *S. aureus*. However, results of antibacterial assays strongly supported the antibacterial effect of HAP/CS/Gr/Gent as opposed to HAP/CS/Gr coating that could not exhibit synergistic antibacterial effect of chitosan and graphene, since concentrations were too low. On the micro level, composite

HAP/CS/Gr and HAP/CS/Gr/Gent exhibited uniform, homogenous surface, with no cracks. The morphology of the coatings was unaffected by gentamicin incorporation, but its presence induced smaller crystallite domain size for HAP/CS/Gr/Gent coating (311 Å) with respect to HAP/CS/Gr coating (435 Å) which is advantageous from bioactivity standpoint. FTIR analysis confirmed the hydrogen bonding between hydroxyl groups of HAP with hydroxyl and amino groups of CS. Moreover, the deconvolution of particular FTIR bands confirmed the "AB-type" substitution of HAP, based on the presence and positions of carbonate bands. Deconvolution of XPS high-resolution C 1s peak gave strong evidence of gentamicin binding to the polymer/graphene network. XPS analysis confirmed the non-stoichiometric HAP with Ca/P ratio of 1.26 and 1.27 for HAP/CS/Gr and HAP/CS/Gr/Gent, respectively, supporting the FTIR results. Thermal stability investigations (TG and DTG curves) showed good thermal properties with weight loss 10.5 wt % and 14.8 wt % for HAP/CS/Gr and HAP/CS/Gr/Gent coatings, respectively. However, only a slight increase in weight loss after gentamicin addition was noticed, as expected. The biocompatibility, investigated by MTT tests was confirmed for HAP/CS/Gr coating, while HAP/CS/Gr/Gent expressed slight cytotoxicity.

In conclusion, based on all characterization results and biological behavior, HAP/CS/Gr/Gent composite coating could be considered as powerful coating material for future use as part of orthopedic implants.

ACKNOWLEDGMENTS

This work was supported by the Ministry of Education, Science and Technological Development, Republic of Serbia (Grant No. III 45019) and the Basic Science Research Program of the Ministry of Education, Science and Technology of Korea [grant number 2018R1A2B5A02023190].

REFERENCES:

1. Yılmaz E, Çakıroğlu B, Gökçe A, Findik F, Gulsoy HO, Gulsoy N, Mutlu Ö, Özacar M. Novel hydroxyapatite/graphene oxide/collagen bioactive composite coating on Ti16Nb alloys by electrodeposition. Mater Sci Eng C. 2019;101:292–305.
2. Özcan M, Hämmerle C. Titanium as a reconstruction and implant material in dentistry: Advantages and pitfalls. Materials (Basel). 2012;5:1528–45.
3. Avcu E, Baştan FE, Abdullah HZ, Rehman MAU, Avcu YY, Boccaccini AR. Electrophoretic deposition of chitosan-based composite coatings for biomedical applications: A review. Prog Mater Sci. 2019;103:69–108.
4. Geuli O, Metoki N, Zada T, Reches M, Eliaz N, Mandler D. Synthesis, Coating and Drug-Release of Hydroxyapatite Nanoparticles Loaded with Antibiotics. J Mater Chem B. 2017;5:7819–30.
5. Sarkar SK, Lee BT. Hard tissue regeneration using bone substitutes: An update on innovations in materials. Korean J Intern Med. 2015;30:279–93.
6. Patel PP, Buckley C, Taylor BL, Sahyoun CC, Patel SD, Mont AJ, Mai L, Patel S, Freeman JW. Mechanical and biological evaluation of a hydroxyapatite-reinforced scaffold for bone regeneration. J Biomed Mater Res - Part A. 2019;107:732–41.
7. Qu H, Fu H, Han Z, Sun Y. Biomaterials for bone tissue engineering scaffolds: A review. RSC Adv. 2019;9:26252–62.
8. Tiplea R, Albu-Kaya MG, Sonmez M, Ghica M, Ficai D, Ficai A, Ardelean IL, Dragos G, Andronescu E. Collagen/hydroxyapatite composite supports for bone tissue engineering. Proceedings of the 3rd World Congress on New Technologies (NewTech'17). 2017;2016–8.
9. Maji K, Dasgupta S. Characterization and in vitro evaluation of gelatin-chitosan scaffold reinforced with bioceramic nanoparticles for bone tissue engineering. J Mater Res. 2019;34:2807–18.
10. Ucar S, Bjørnøy SH, Bassett DC, Strand BL, Sikorski P, Andreassen JP. Formation of Hydroxyapatite via Transformation of Amorphous Calcium Phosphate in the Presence of Alginate Additives. Cryst Growth Des. 2019;19:7077–87.
11. Januariyasa IK, Ana ID, Yusuf Y. Nanofibrous poly(vinyl alcohol)/chitosan contained carbonated hydroxyapatite nanoparticles scaffold for bone tissue engineering. Mater Sci Eng C. 2020; 107; Article ID 110347.
12. Yadav M, Rhee KY, Park SJ, Hui D. Mechanical properties of Fe_3O_4/GO/chitosan composites. Compos Part B Eng. 2014;66:89–96.
13. Guo L, Du Z, Wang Y, Cai Q, Yang X. Degradation behaviors of three-dimensional hydroxyapatite fibrous scaffolds stabilized by different biodegradable polymers. Ceram Int. 2020; doi.org/10.1016/j.ceramint.2020.02.217
14. Liu Y, Wang R, Chen S, Xu Z, Wang Q, Yuan P, Zhou Y, Zhang Y, Chen J. Heparan sulfate loaded polycaprolactone-hydroxyapatite scaffolds with 3D printing for bone defect repair. Int J Biol Macromol. 2020;148:153–62.
15. Takahashi M, Yamaguchi M, Tanimoto Y, Yao-Umezawa E, Kasai K. Biological evaluation of a prototype material made of polyglycolic acid and hydroxyapatite. J Hard Tissue Biol. 2015;24:375–84.
16. Behera K, Sivanjineyulu V, Chang YH, Chiu FC. Thermal properties, phase morphology and stability of biodegradable PLA/PBSL/HAp composites. Polym Degrad Stab. 2018;154:248–60.
17. Zhang R, Hu H, Liu Y, Tan J, Chen W, Ying C, Liu Q, Fu X, Hu S, Wong CP. Homogeneously dispersed composites of hydroxyapatite nanorods and poly(lactic acid) and their mechanical properties and crystallization behavior. Compos Part A-Appl S. 2020;132; Article ID 105841.
18. Stevanović M, Đošić M, Janković A, Kojić V, Vukašinović-Sekulić M, Stojanović J, Odović J, Crevar Sakač M, Rhee KY, Mišković-Stanković V. Gentamicin-Loaded Bioactive Hydroxyapatite/Chitosan Composite Coating Electrodeposited on Titanium. ACS Biomater Sci Eng. 2018;4:3994–4007.
19. Hurt AP, Kotha AK, Trivedi V, Coleman NJ. Bioactivity , biocompatibility and antimicrobial properties of a chitosan-mineral composite for periodontal tissue regeneration. Polimeros. 2015;25:311–6.
20. Francis Suh JK, Matthew HWT. Application of chitosan-based polysaccharide biomaterials in cartilage tissue engineering: A review. Biomaterials. 2000;21:2589–98.
21. Candy T, Sharma CP. Chitosan -as a biomaterial. Biohat, Art Cells, Art Org. 1990;18:1–24.

22. VenkatesanaJ, Lowe B, Pallela R, Kima and Kim S.-K. Chitosan-Based Polysaccharide Biomaterials. Polysaccharides 2014; doi:10.1007/978-3-319-03751-6_25-1
23. Shi YY, Li M, Liu Q, Jia ZJ, Xu XC, Cheng Y, Zheng YF. Electrophoretic deposition of graphene oxide reinforced chitosan–hydroxyapatite nanocomposite coatings on Ti substrate. J Mater Sci Mater Med. 2016;27:1–13.
24. Mohan Raj R, Priya P, Raj V. Gentamicin-loaded ceramic-biopolymer dual layer coatings on the Ti with improved bioactive and corrosion resistance properties for orthopedic applications. J Mech Behav Biomed Mater. 2018;82:299–309.
25. Qu Y, He F, Yu C, Liang X, Liang D, Ma L, Zhang Q, Lv J, Wu J. Advances on graphene-based nanomaterials for biomedical applications. Mater Sci Eng C. 2018;90:764–80.
26. Yadav M, Rhee KY, Jung IH, Park SJ. Eco-friendly synthesis, characterization and properties of a sodium carboxymethyl cellulose/graphene oxide nanocomposite film. Cellulose. 2013;20:687–98.
27. Li D, Liu T, Yu X, Wu D, Su Z. Fabrication of graphene-biomacromolecule hybrid materials for tissue engineering application. Polym Chem. 2017;8:4309–21.
28. Liao C, Li Y, Tjong SC. Graphene Nanomaterials: Synthesis, Biocompatibility, and Cytotoxicity. Int J Mol Sci. 2018;19:3564–600.
29. Spriano S, Yamaguchi S, Baino F, Ferraris S. A critical review of multifunctional titanium surfaces: New frontiers for improving osseointegration and host response, avoiding bacteria contamination. Acta Biomater. 2018;79:1–22.
30. Croes M, Bakhshandeh S, van Hengel IAJ, Lietaert K, van Kessel KPM, Pouran B, van der Wal BCH, Vogely HC, Van Hecke W, Fluit AC, Boel CHE, Alblas J, Zadpoor AA, Weinans H, Amin Yavari S. Antibacterial and immunogenic behavior of silver coatings on additively manufactured porous titanium. Acta Biomater. 2018;81:315–27.
31. Ordikhani F, Farani MR, Dehghani M, Tamjid E, Simchi A. Physicochemical and biological properties of electrodeposited graphene oxide/chitosan films with drug-eluting capacity. Carbon. 2015;84:91–102.
32. Stigter M, Bezemer J, De Groot K, Layrolle P. Incorporation of different antibiotics into carbonated hydroxyapatite coatings on titanium implants, release and antibiotic efficacy. J Control Release. 2004;99:127–37.
33. Patel KD, Singh RK, Lee EJ, Han CM, Won JE, Knowles JC, Kim HW. Tailoring solubility and drug release from electrophoretic deposited chitosan-gelatin films on titanium. Surf Coat Tech. 2014;242:232–6.
34. Clifford A, Zhitomirsky I. Aqueous electrophoretic deposition of drugs using bile acids as solubilizing, charging and film-forming agents. Mater Lett. 2018;227:1–4.
35. Chen Q, Cabanas-Polo S, Ding YP, Boccaccini AR. Bioactive Glass-Biopolymer Multilayer Coatings Fabricated by Electrophoretic Deposition Combined with Layer-by-Layer Assembly. Key Eng Mater. 2015;654:170–5.
36. Pan X, Chen S, Li D, Rao W, Zheng Y, Yang Z, Li L, Guan X, Chen Z. The synergistic antibacterial mechanism of gentamicin-loaded $CaCO_3$ nanoparticles. Front Chem. 2018;5:1–9.
37. Tang S, Tian B, Ke QF, Zhu ZA, Guo YP. Gentamicin-loaded carbonated hydroxyapatite coatings with hierarchically porous structures: Drug delivery properties, bactericidal properties and biocompatibility. RSC Adv. 2014;40:41500–9.
38. Services H, Goode J, Services H. Use of International Standard ISO 10993-1, Biological evaluation of medical devices - Part 1: Evaluation and testing within a risk management process. U.S. Department of Health and Human Services Food and Drug Administration; 2016.
39. Ballarre J, Aydemir T, Liverani L, Roether JA, Goldmann WH, Boccaccini AR. Versatile bioactive and antibacterial coating system based on silica, gentamicin, and chitosan: Improving early stage performance of titanium implants. Surf Coatings Technol. 2020;381; Article ID 125138.
40. Tian B, Tang S, Wang CD, Wang WG, Wu CL, Guo YJ, Guo YP, Zhu ZA. Bactericidal properties and biocompatibility of a gentamicin-loaded Fe_3O_4/carbonated hydroxyapatite coating. Colloid Surface B. 2014;123:403–12.
41. Pishbin F, Mouriño V, Flor S, Kreppel S, Salih V, Ryan MP, Boccaccini AR. Electrophoretic Deposition of Gentamicin-Loaded Bioactive Glass/Chitosan Composite Coatings for Orthopaedic Implants. ACS Appl Mater Interfaces. 2014;6:8796–806.

42. Zhitomirsky I, Hashambhoy A. Chitosan-mediated electrosynthesis of organic – inorganic nanocomposites. J Mater Process Technol. 2007;191:68–72.
43. Đošić M, Eraković S, Janković A, Vukašinović-Sekulić M, Matić IZ, Stojanović J, Rhee KY, Mišković-Stanković V, Park SJ. In vitro investigation of electrophoretically deposited bioactive hydroxyapatite/chitosan coatings reinforced by graphene. J Ind Eng Chem. 2017;47:336–47.
44. Geetha V, Gomathi T, Sudha PN. Preparation and characterization of Graphene-grafted- chitosan / hydroxyapatite composite. J Chem Pharm Res. 2015;7:871–6.
45. Janković A, Eraković S, Vukašinović-Sekulić M, Mišković-Stanković V, Park SJ, Rhee KY. Graphene-based antibacterial composite coatings electrodeposited on titanium for biomedical applications. Prog Org Coat. 2015;83:1–10.
46. Ren F, Ding Y, Leng Y. Infrared spectroscopic characterization of carbonated apatite: A combined experimental and computational study. J Biomed Mater Res A. 2014;102:496–505.
47. Brangule A, Gross KA. Importance of FTIR Spectra Deconvolution for the Analysis of Amorphous Calcium Phosphates. IOP Conference Series: Materials Science and Engineering. 2015;77; Article ID 012027.
48. Yang W, Xi X, Li J, Cai K. Comparison of crystal structure between carbonated hydroxyapatite and natural bone apatite with theoretical calculation. Asian J Chem. 2013;25:3673–8.
49. Mayo D, Miller F, Hannah R. Course Notes On The Interpretation Of Infrared And Raman Spectra. Hoboken, New Jersey: John Wiley and Sons Ltd; 2004. 567 p.
50. Xu YX, Kim KM, Hanna MA, Nag D. Chitosan-starch composite film: Preparation and characterization. Ind Crops Prod. 2005;21:185–92.
51. Zhang K, Peschel D, Helm J, Groth T, Fischer S. FT Raman investigation of novel chitosan sulfates exhibiting osteogenic capacity. Carbohydr Polym. 2011;83:60–5.
52. Surudžić R, Janković A, Bibić NN, Vukašinović-Sekulić M, Perić-Grujić A, Mišković-Stanković V, Park SJ, Rhee KY. Physico-chemical and mechanical properties and antibacterial activity of silver/poly(vinyl alcohol)/graphene nanocomposites obtained by electrochemical method. Compos Part B Eng. 2016;85:102–12.
53. Berzina-Cimdina L, Borodajenko N. Research of Calcium Phosphates Using Fourier Transform Infrared Spectroscopy. In: Theophanides T, editor. Infrared Spectroscopy: Materials Science, Engineering and Technology ; London: IntechOpen; 2012. p 123–48.
54. Rapacz-Kmita A, Stodolak-Zych E, Ziabka M, Rozycka A, Dudek M. Instrumental characterization of the smectite clay-gentamicin hybrids. B Mater Sci. 2015;38:1069–78.
55. Nikpour MR, Rabiee SM, Jahanshahi M. Synthesis and characterization of hydroxyapatite/chitosan nanocomposite materials for medical engineering applications. Compos Part B Eng. 2012;43:1881–6.
56. Djošić MS, Mitrić M, Mišković-Stankovic VB. The porosity and roughness of electrodeposited calcium phosphate coatings in simulated body fluid. J Serb Chem Soc. 2015;80:237–51.
57. Okada M, Matsumoto T. Synthesis and modification of apatite nanoparticles for use in dental and medical applications. Jpn Dent Sci Rev. 2015;51:85–95.
58. Zhang S, Cheng X, Shi J, Pang J, Wang Z, Shi W, Liu F, Ji B. Electrochemical deposition of calcium phosphate/chitosan/gentamicin on a titanium alloy for bone tissue healing. Int J Electrochem Sci. 2018;13:4046–54.
59. Han C, Yao Y, Cheng X, Luo J, Luo P, Wang Q, Yang F, Wei Q, Zhang Z. Electrophoretic Deposition of Gentamicin-Loaded Silk Fibroin Coatings on 3D-Printed Porous Cobalt-Chromium-Molybdenum Bone Substitutes to Prevent Orthopedic Implant Infections. Biomacromolecules. 2017;18:3776–87.
60. Thomas MB, Metoki N, Mandler D, Eliaz N. In Situ Potentiostatic Deposition of Calcium Phosphate with Gentamicin-Loaded Chitosan Nanoparticles on Titanium Alloy Surfaces. Electrochim Acta. 2016;222:355–60.
61. Zhang J, Wen Z, Zhao M, Li G, Dai C. Effect of the addition CNTs on performance of CaP/chitosan/coating deposited on magnesium alloy by electrophoretic deposition. Mater Sci Eng C. 2016;58:992–1000.
62. Fan Z, Wang J, Wang Z, Li Z, Qiu Y, Wang H, Xu Y, Niu L, Gong P, Yang S. Casein phosphopeptide-biofunctionalized graphene biocomposite for hydroxyapatite biomimetic mineralization. J Phys Chem C. 2013;117:10375–82.

63. Li M, Wang Y, Liu Q, Li Q, Cheng Y, Zheng Y, Xi T, Wei S. In situ synthesis and biocompatibility of nano hydroxyapatite on pristine and chitosan functionalized graphene oxide. J Mater Chem B. 2013;1:475–84.
64. Degoutin S, Jimenez M, Chai F, Pinalie T, Bellayer S, Vandenbossche M, Neut C, Blanchemain N, Martel B. Simultaneous immobilization of heparin and gentamicin on polypropylene textiles: A dual therapeutic activity. J Biomed Mater Res A. 2014;102:3846–54.
65. Liu Y, Ji P, Lv H, Qin Y, Deng L. Gentamicin modified chitosan film with improved antibacterial property and cell biocompatibility. Int J Biol Macromol. 2017;98:550–6.
66. Francis L, Meng D, Knowles J, Keshavarz T, Boccaccini AR, Roy I. Controlled delivery of gentamicin using poly(3-hydroxybutyrate) microspheres. Int J Mol Sci. 2011;12:4294–314.
67. Kazuki Igeta, Yuta Kuwamura, Naohiro Horiuchi, Kosuke Nozaki, Daichi Shiraishi, Mamoru Aizawa, Kazuaki Hashimoto, Kimihiro Yamashita AN. Morphological and functional changes in RAW264 macrophage-like cells in response to a hydrated layer of carbonate-substituted hydroxyapatite. J Biomed Mater Res A. 2008;105:1063–70.
68. Sakae T, Ookubo A, LeGeros RZ, Shimogoryou R, Sato Y, Lin S, Yamamoto H, Kozawa Y. Bone formation induced by several carbonate- and fluoride-containing apatite implanted in dog mandible. Key Eng Mater. 2003;240–242:395–8.
69. Li M, Liu Q, Jia Z, Xu X, Shi Y, Cheng Y, Zheng Y, Xi T, Wei S. Electrophoretic deposition and electrochemical behavior of novel graphene oxide-hyaluronic acid-hydroxyapatite nanocomposite coatings. Appl Surf Sci. 2013;284:804–10.
70. Hanuza J, Wandas M, Dymin L. Molecular and Biomolecular Spectroscopy Determination of N-acetylation degree in chitosan using Raman spectroscopy. Spectrochim Acta Part A. 2015;134:114–20.
71. Childres I, Jauregui L, Park W, Cao H, Chen Y. Raman Spectroscopy of Graphene and Related Materials. In: Jang JI editor. New Developments in Photon and Materials Research. New York: NOVA Science Publishers;2013. p 403–418.
72. El-Hefian EA, Elgannoudi ES, Mainal A, Yahaya AH. Characterization of chitosan in acetic acid: Rheological and thermal studies. Turkish J Chem. 2010;34:47–56.
73. Dwivedi C, Pandey H, Pandey AC, Ramteke PW. Novel Gentamicin Loaded Electrospun Nanofibrous Scaffolds for Wound Healing: an in -vitro Study. Int J Pharm Sci Res. 2013;4:2230–3.
74. Patel KD, El-Fiqi A, Lee HY, Singh RK, Kim D-AA, Lee HH, Kim H-WW. Chitosan-nanobioactive glass electrophoretic coatings with bone regenerative and drug delivering potential. J Mater Chem. 2012;22:24945–56.
75. Janković A, Eraković S, Mitrić M, Matić IZ, Juranić ZD, Tsui GCP, Tang CY, Mišković-Stanković V, Rhee KY, Park SJ. Bioactive hydroxyapatite/graphene composite coating and its corrosion stability in simulated body fluid. J Alloys Compd. 2015;624:148–57.
76. Loryuenyong V, Totepvimarn K, Eimburanapravat P, Boonchompoo W, Buasri A. Preparation and characterization of reduced graphene oxide sheets via water-based exfoliation and reduction methods. Adv Mater Sci Eng. 2013;Article ID 923403, 1-5.
77. Dwivedi C, Pandey H, Pandey AC, Ramteke PW. Fabrication and Assessment of Gentamicin Loaded Electrospun Nanofibrous Scaffolds as a Quick Wound Healing Dressing Material. Curr Nanosci. 2015;11:222–8.
78. Ivanova TI, Frank-Kamenetskaya OV, Kol'tsov AB, Ugolkov VL. Crystal Structure of Calcium-Deficient Carbonated Hydroxyapatite. Thermal Decomposition. J Solid State Chem. 2001;160:340–9.
79. Pandey H, Parashar V, Parashar R, Prakash R, Ramteke PW, Pandey AC. Controlled drug release characteristics and enhanced antibacterial effect of graphene nanosheets containing gentamicin sulfate. Nanoscale. 2011;3:4104–8.
80. Tangy F, Moukkadem M, Vindimian E, Capmau ML, Le Goffic F. Mechanism of action of gentamicin components: Characteristics of their binding to Escherichia coli ribosomes. Eur J Biochem. 1985;147:381–6.
81. Yoshizawa S. Structural origins of gentamicin antibiotic action. EMBO J. 1998;17:6437–48.
82. Hahn FE, Sarre SG. Mechanism of Action of Gentamicin. J Infect Dis. 2016;119:364–9.
83. Milanesi G, Ciferri O. Studies on the Mechanism of Action of Gentamicin. Effect on Protein Synthesis in Cell-Free Extracts of Escherichia coli. Biochemistry. 1966;5:3926–35.

84. Rabea EI, Badawy MET, Stevens CV, Smagghe G, Steurbaut W. Chitosan as antimicrobial agent: Applications and mode of action. Biomacromolecules. 2003;4:1457–65.
85. Ji H, Sun H, Qu X. Antibacterial applications of graphene-based nanomaterials : Recent achievements and challenges. Adv Drug Deliv Rev. 2016;105:176–89.
86. Pankey GA, Sabath LD. Clinical Relevance of Bacteriostatic versus Bactericidal Mechanisms of Action in the Treatment of Gram-Positive Bacterial Infections. Clin Infect Dis. 2004;38:864–70.
87. Sjögren G, Sletten G, Dahl EJ. Cytotoxicity of dental alloys, metals, and ceramics assessed by Millipore filter, agar overlay, and MTT tests. J Prosthet Dent. 2000;84:229–36.

Figure legends

Fig. 1. FTIR spectra of HAP/CS/Gr (a) and HAP/CS/Gr/Gent coating (b); deconvolution of FTIR spectral bands for HAP/CS/Gr coating in the specific regions: carbonate band from 800 to 900 cm^{-1} (c) and 1350 to 1600 cm^{-1} (d); FTIR spectra for HAP/CS/Gr (e) and HAP/CS/Gr/Gent coating (f) in the region from 1500 to 1700 cm^{-1}.

Fig. 2. XRD patterns of (a) HAP/CS/Gr and (b) HAP/CS/Gr/Gent coatings

Fig. 3. XPS spectra for HAP/CS/Gr and HAP/CS/Gr/Gent coatings: C 1s (a,b); O 1s (c,d); N 1s (e,f).

Fig. 4. FE-SEM microphotographs of (a, b) HAP/CS/Gr and (c, d) HAP/CS/Gr/Gent coatings.

Fig. 5. Raman spectra of (a) HAP/CS/Gr and (b) HAP/CS/Gr/Gent coatings.

Fig. 6. TG and DTG curves of (a) HAP/CS/Gr and (b) HAP/CS/Gr/Gent coatings.

Fig. 7. Agar diffusion test for *S. aureus* (a) and *E. coli* (b) in the presence of Gent (control), HAP/CS/Gr (sample 1) and HAP/CS/Gr/Gent (sample 2).

Fig. 8. Reduction of viable cell number of: (a) *S. aureus* and (b) *E. coli* after contact with HAP/CS/Gr and HAP/CS/Gr/Gent coatings for 0, 1, 3 and 24 h in PB as compared to the control samples coatings. Statistical evaluation for samples done in triplicate was performed using one-way ANOVA, with a multiple comparisons posthoc analysis (* $p < 0.01$ for the respective bacteria strain).

Fig. 9. MRC-5 and L929 cell viability for HAP/CS/Gr and HAP/CS/Gr/Gent coatings. Statistical evaluation for samples done in triplicate was performed using one-way ANOVA, with a multiple comparisons posthoc analysis (* $p < 0.01$ within the cell line).

Table 1. Calculated XRD parameters (crystal planes *d*-spacing values)

coating	crystal planes			
	(002)	(211)	(112)	(300)
	d-spacing, Å			
HAP/CS/Gr	3.4537	2.8271	2.7899	2.7326
HAP/CS/Gr/Gent	3.4313	2.8032	2.7695	2.7085

Table 2. Crystallite domain size, unit cell parameters and volume

coating	Parameter			Crystallite domain size, Å
	a, Å	*c*, Å	*V*, Å^3	
HAP/CS/Gr	9.446	6.907	536.1	435
HAP/CS/Gr/Gent	9.383	6.863	523	311

Table 3.Elemental composition of HAP/CS/Gr and HAP/CS /Gr/Gent coatings based on XPS surface analysis.

	HAP/CS/Gr, at %	HAP/CS/Gr/Gent, at %
C 1s	21.0	21.5
O 1s	51.6	51.3
N 1s	1.3	1.2
P 2p	11.6	11.1
Ca 2p	14.6	14.1
S 2p	/	0.7
Ca/P ratio	1.26	1.27

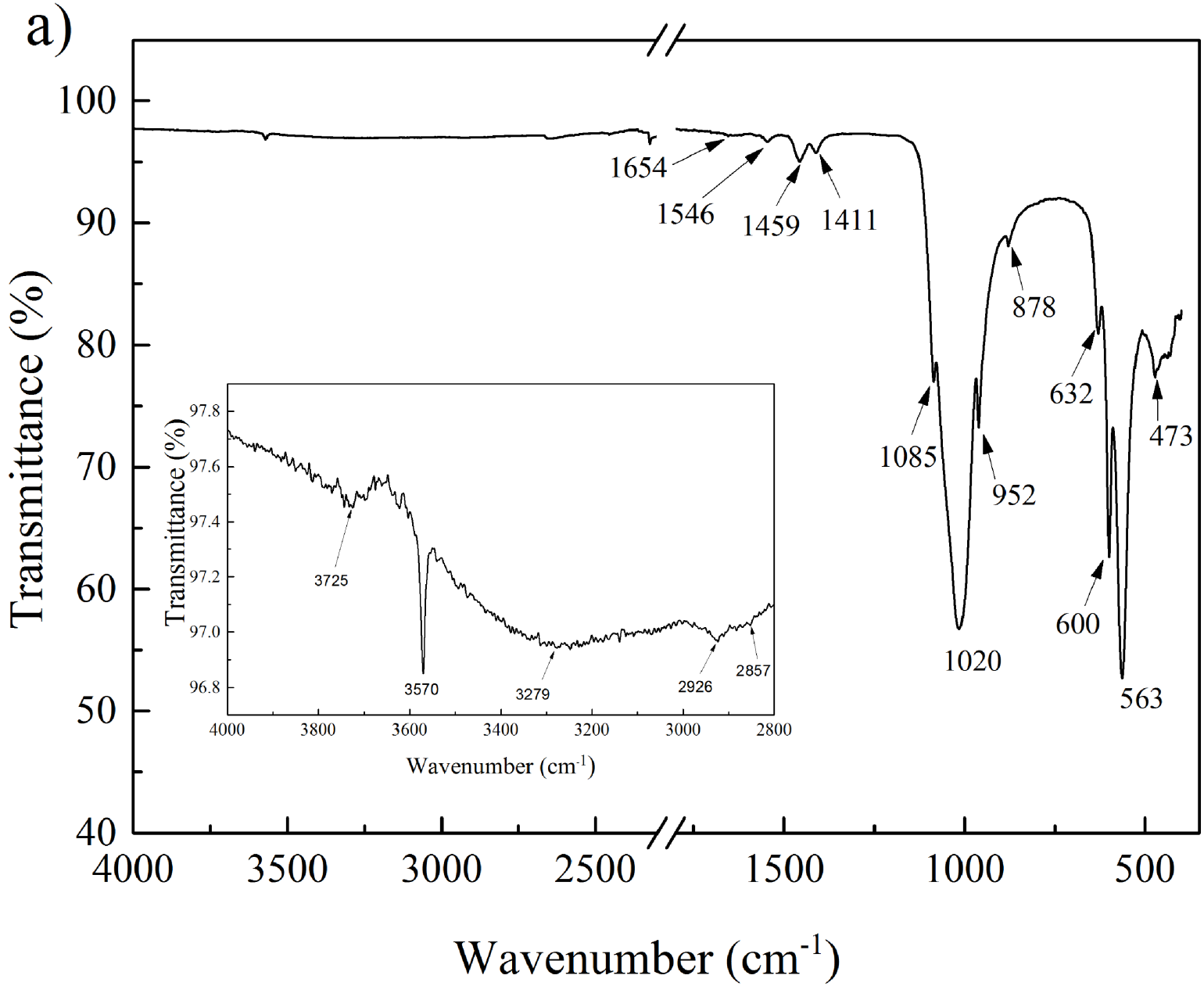

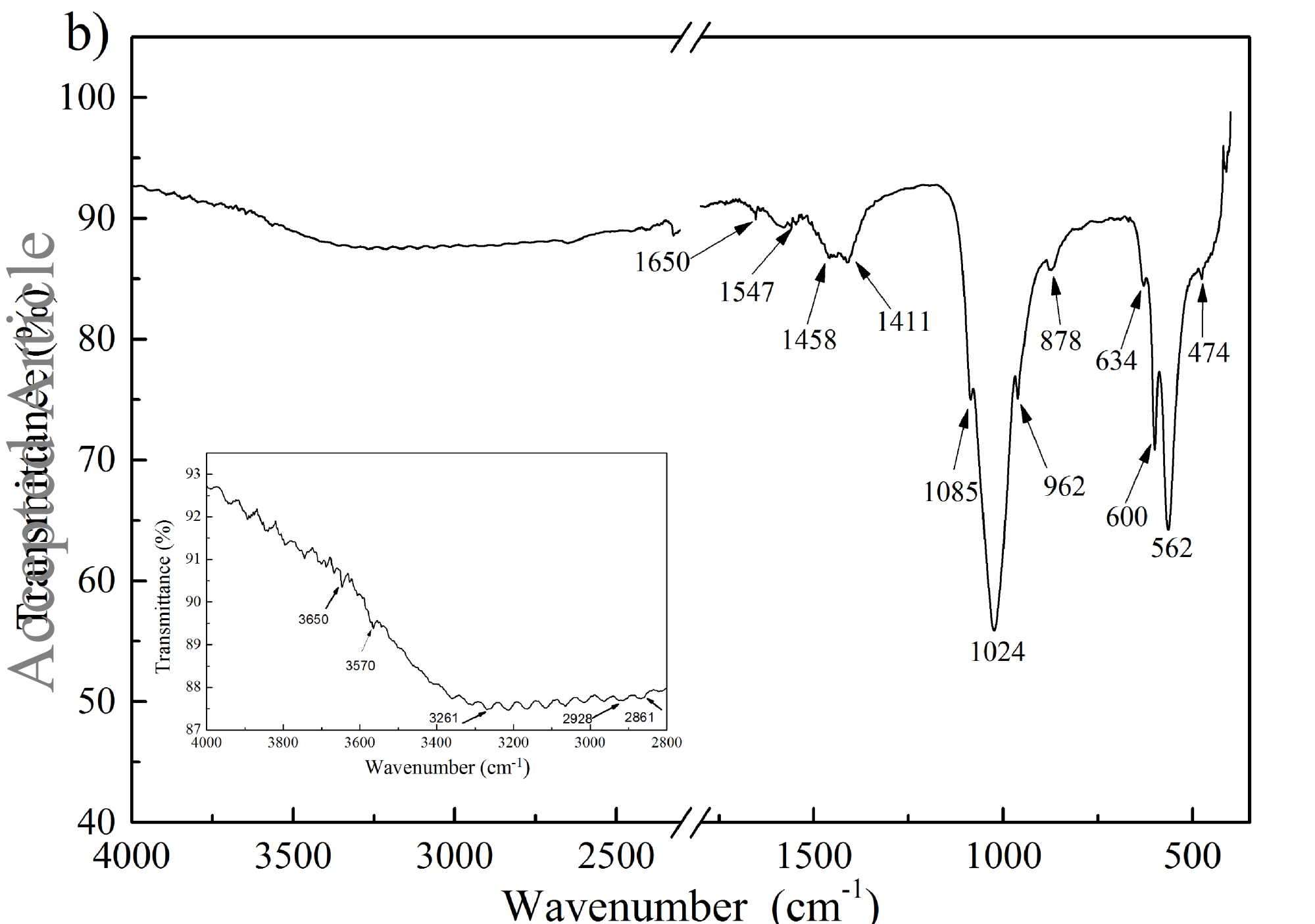
b)
Transmittance (%)
Wavenumber (cm-1)
1650
1547
1458
1411
1085
1024
962
878
634
600
562
474
3650
3570
3261
2928
2861

c)

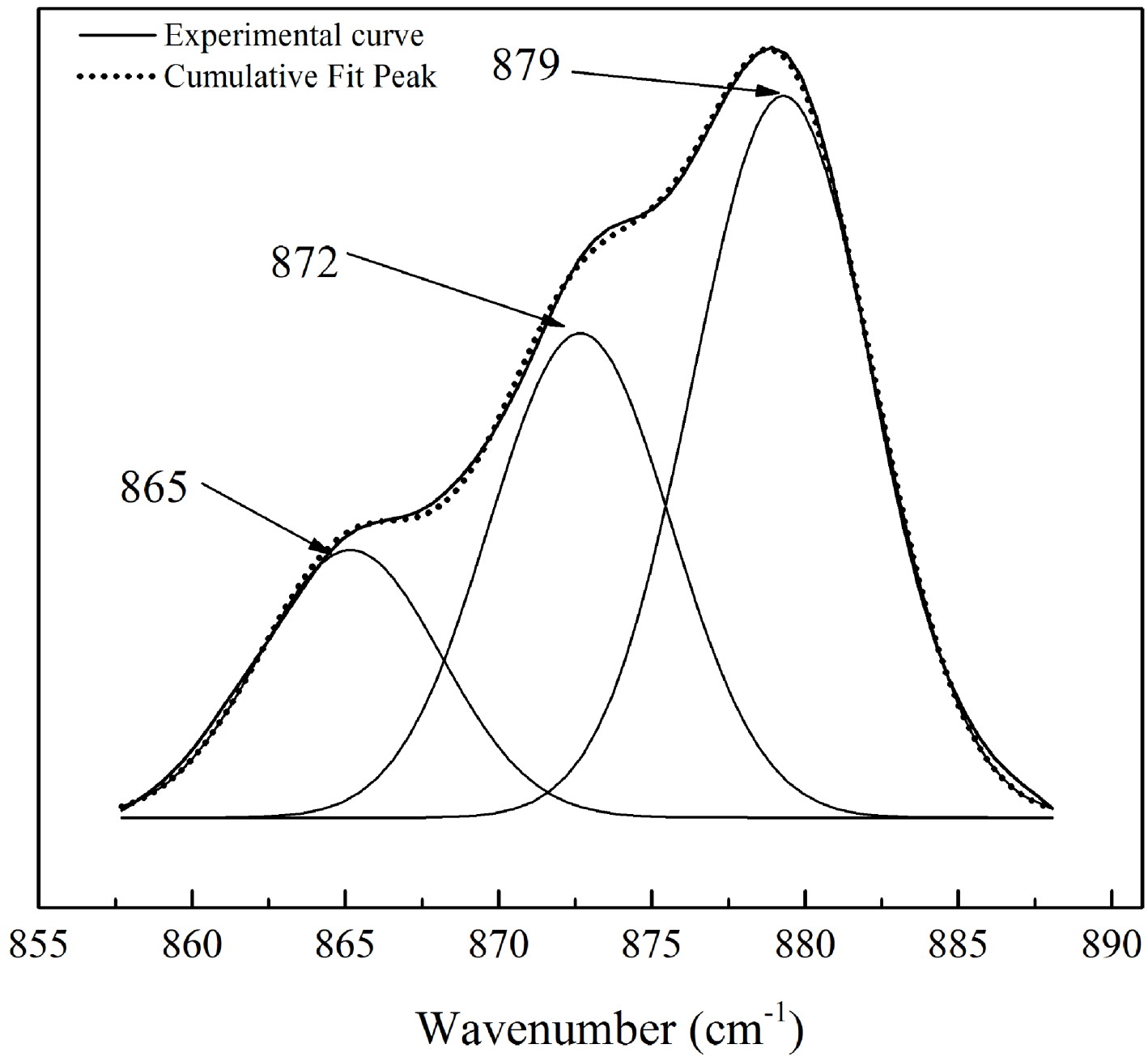

d)

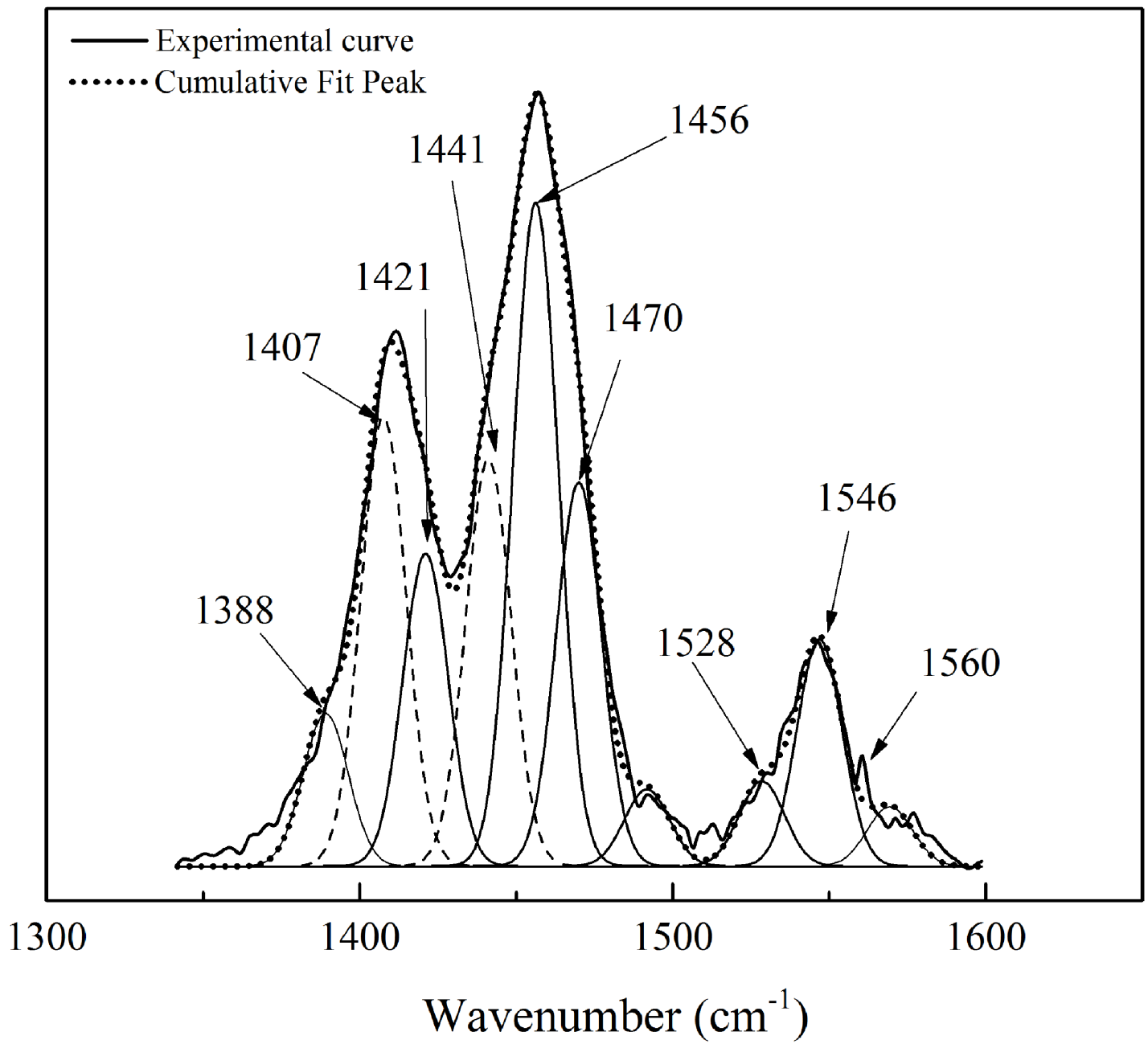

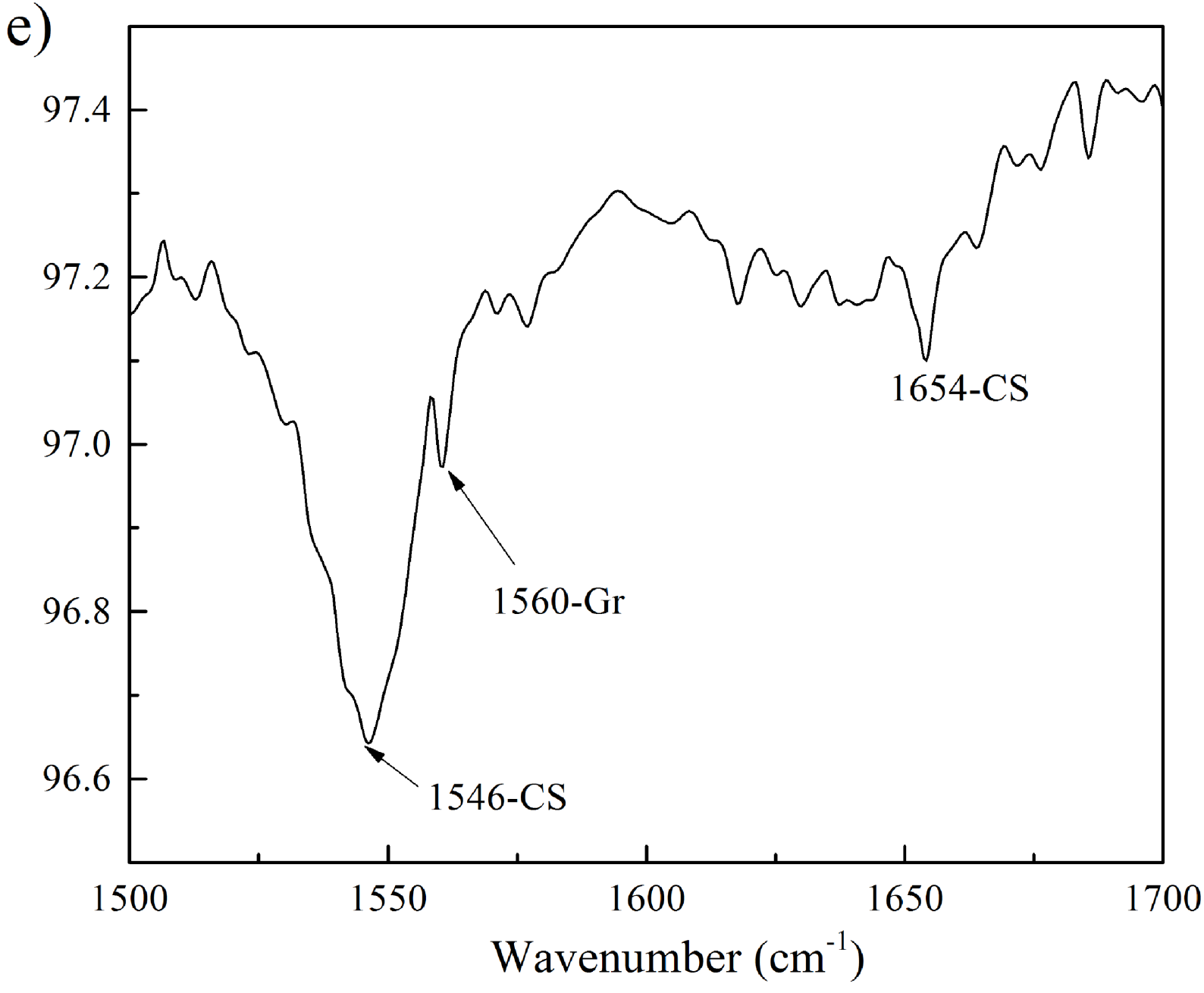

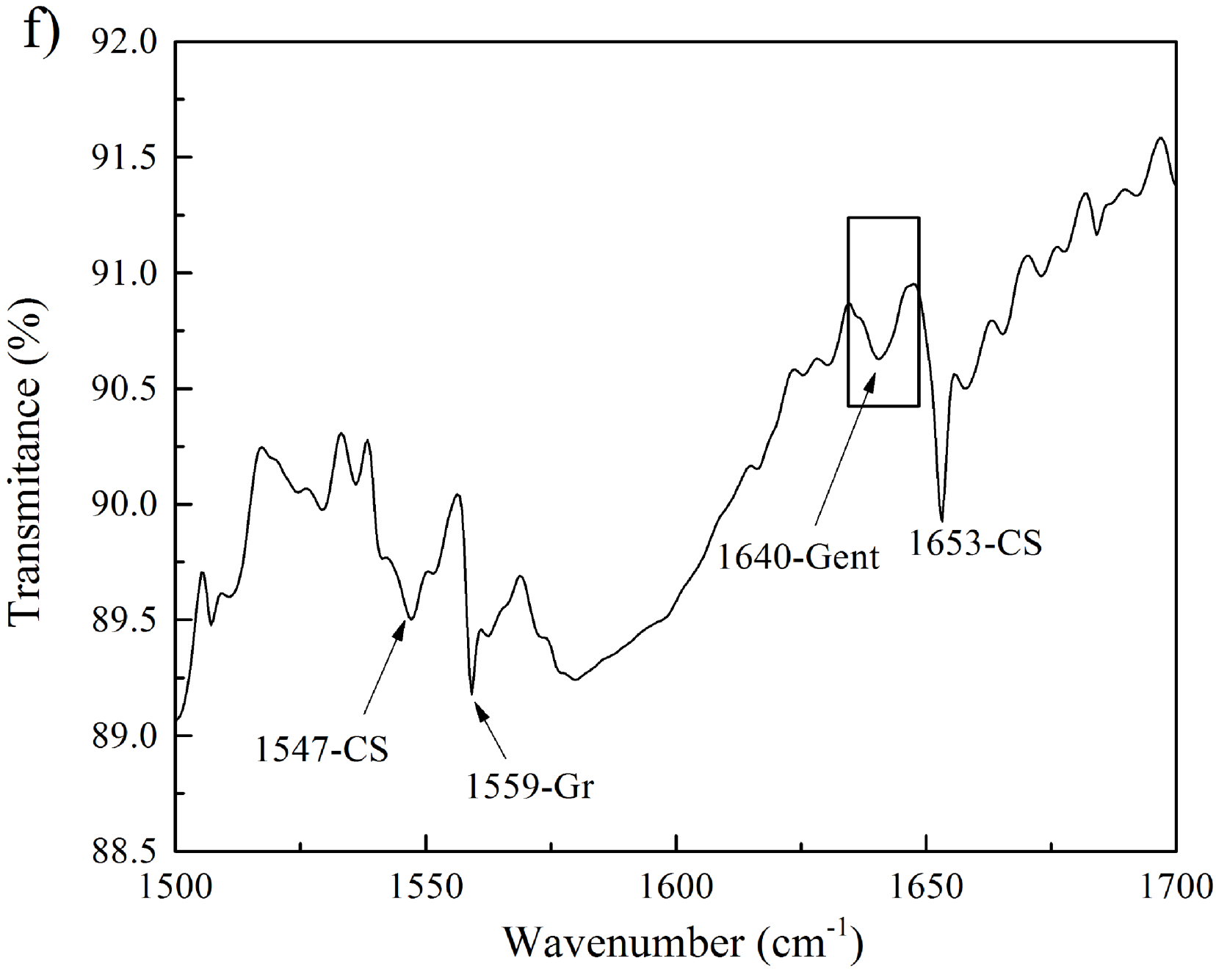

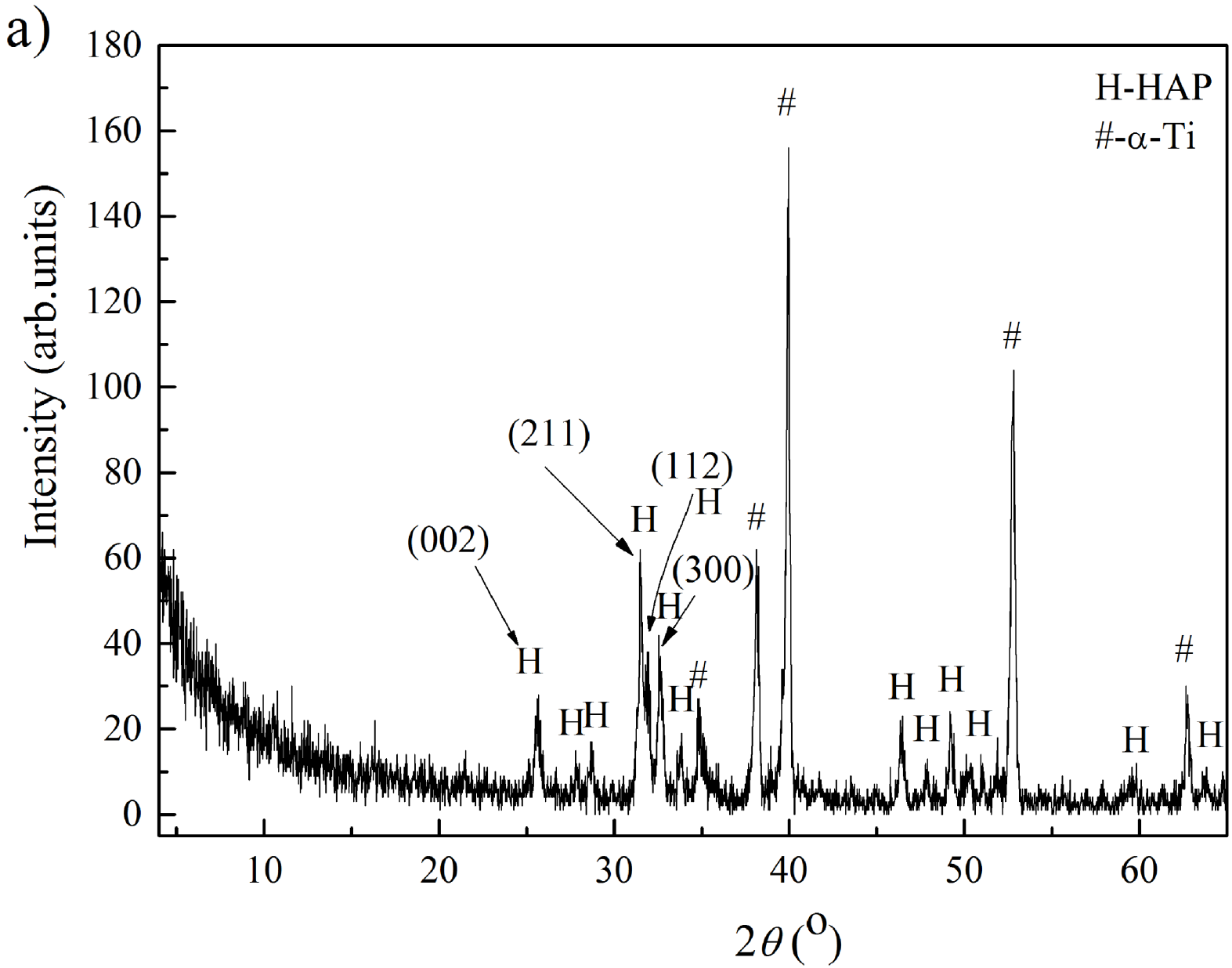

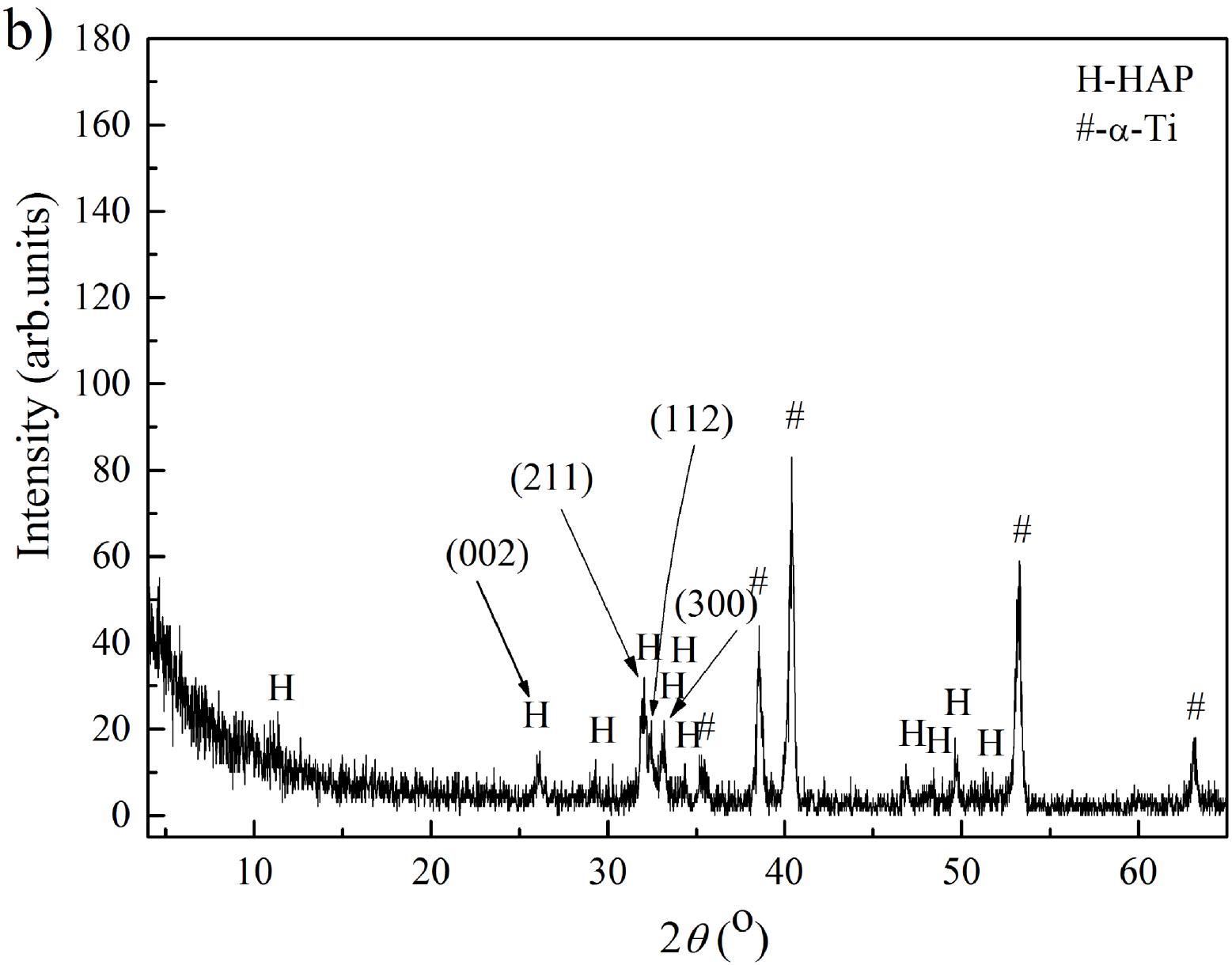

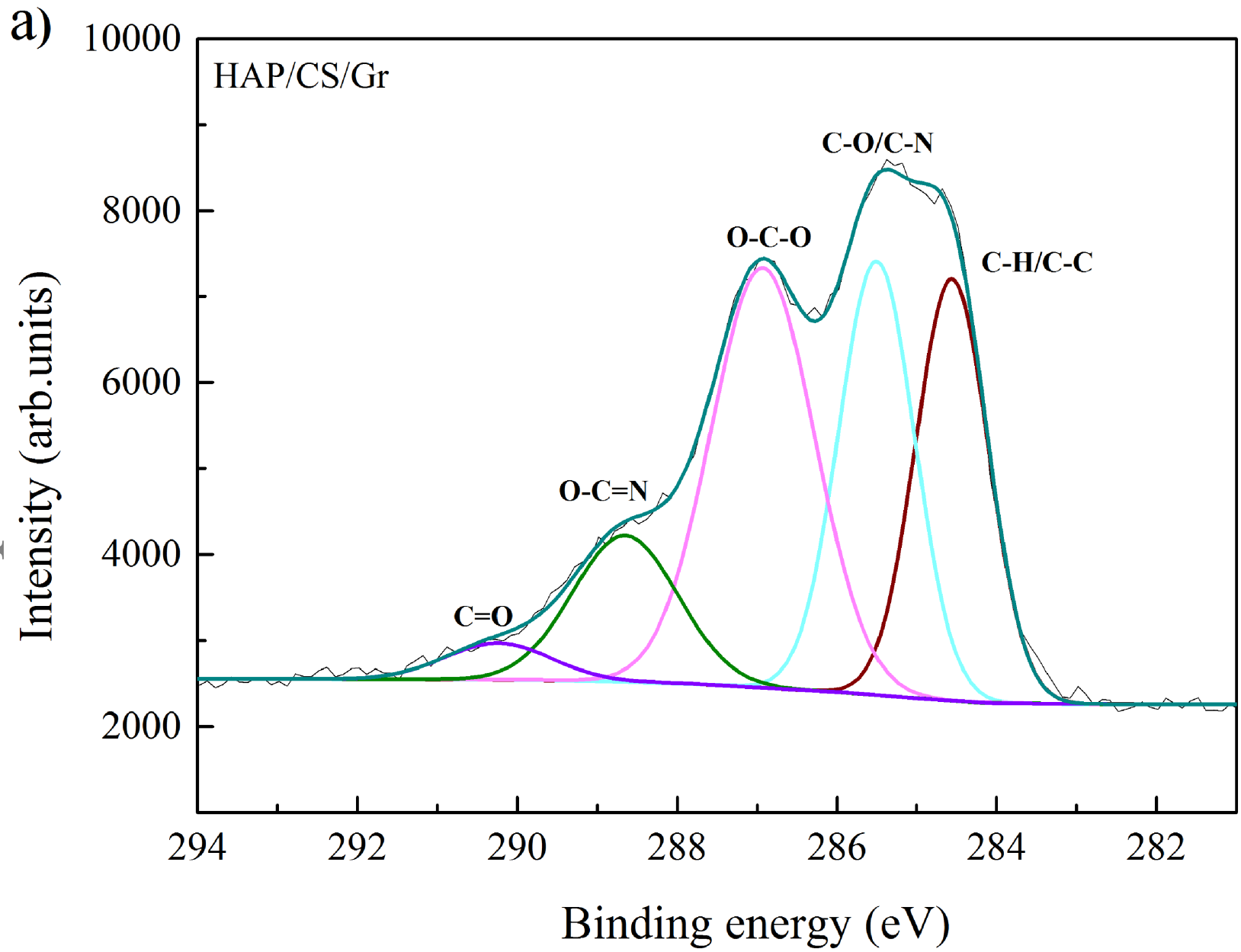

b)

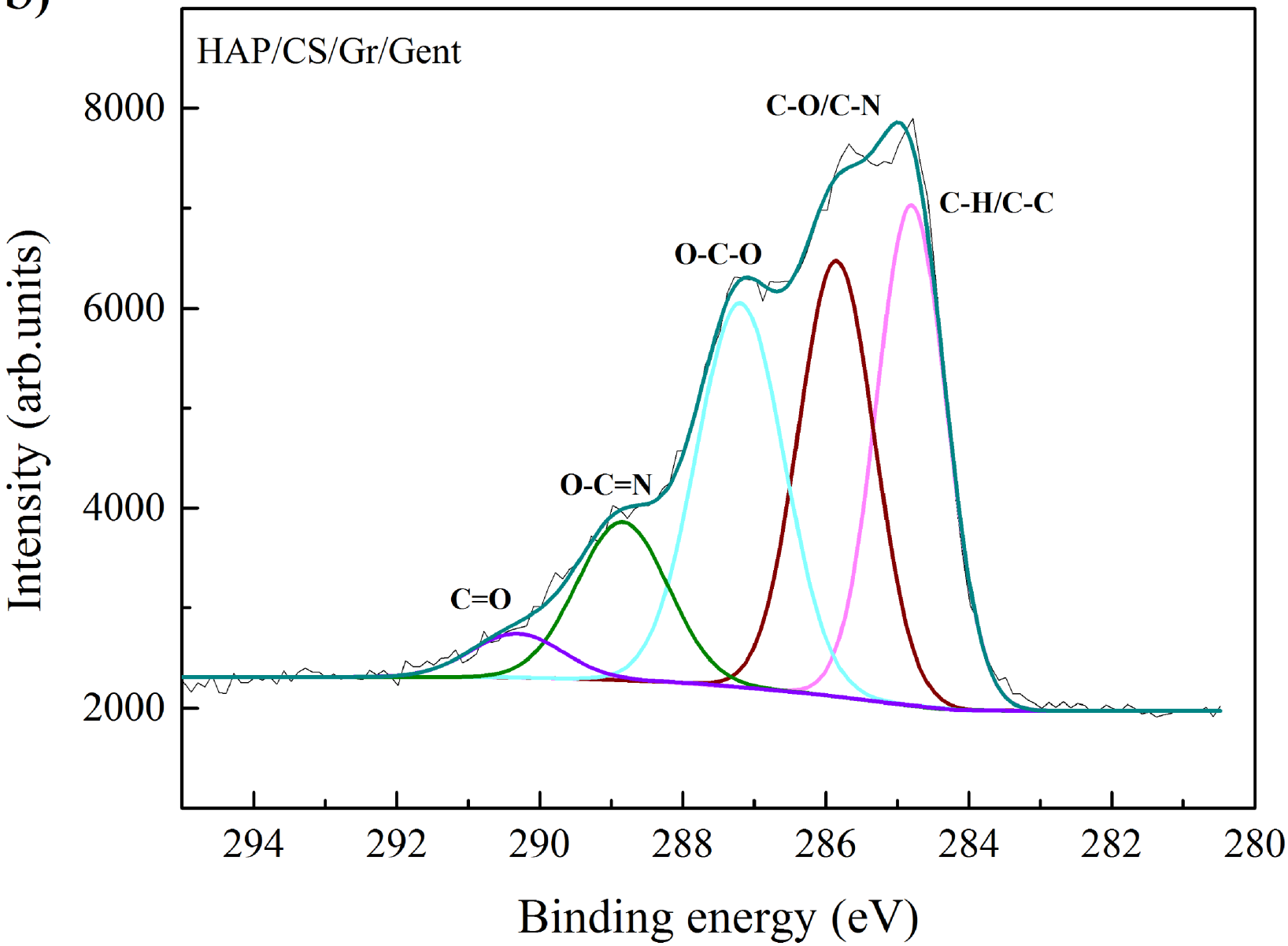

c)

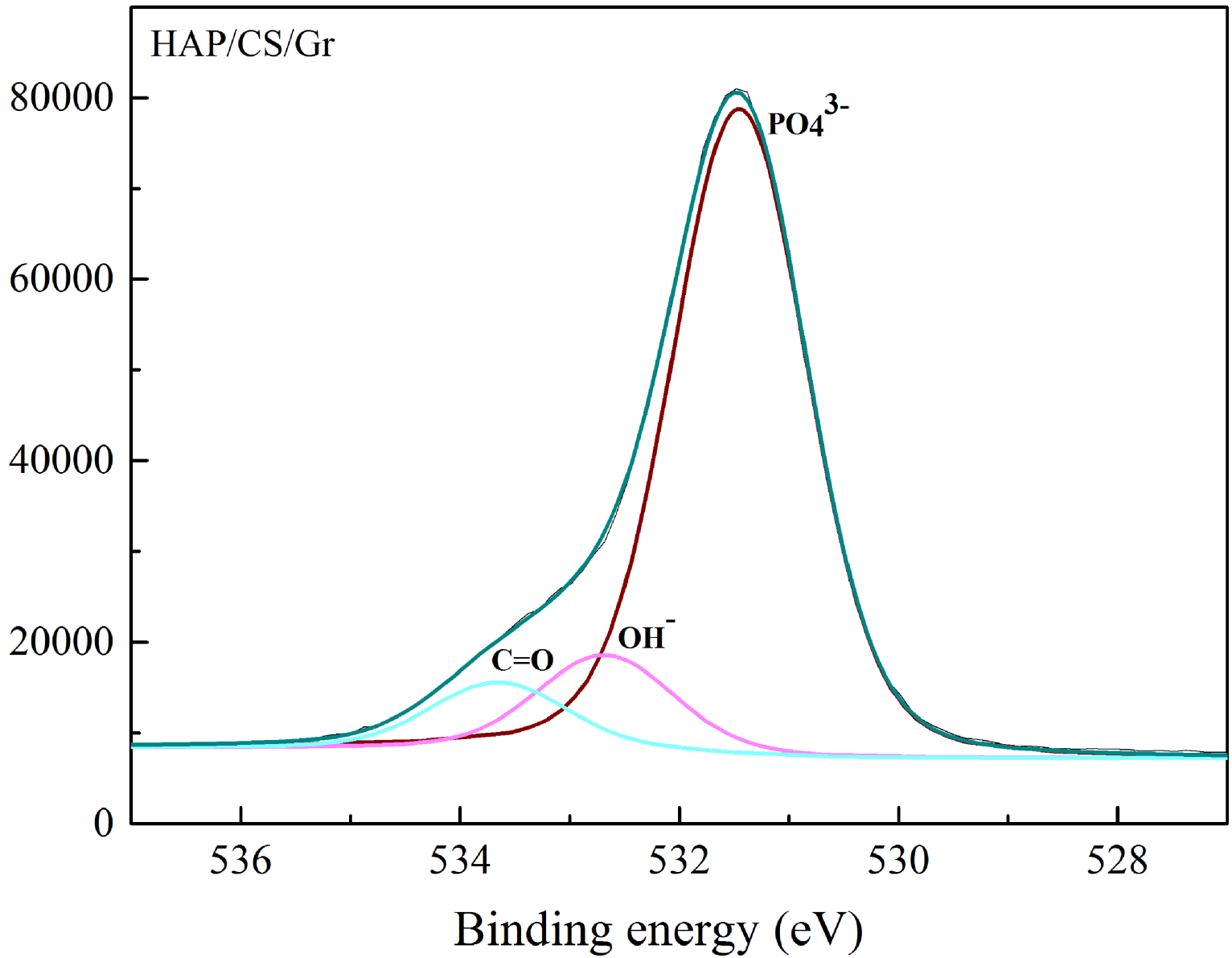

d)

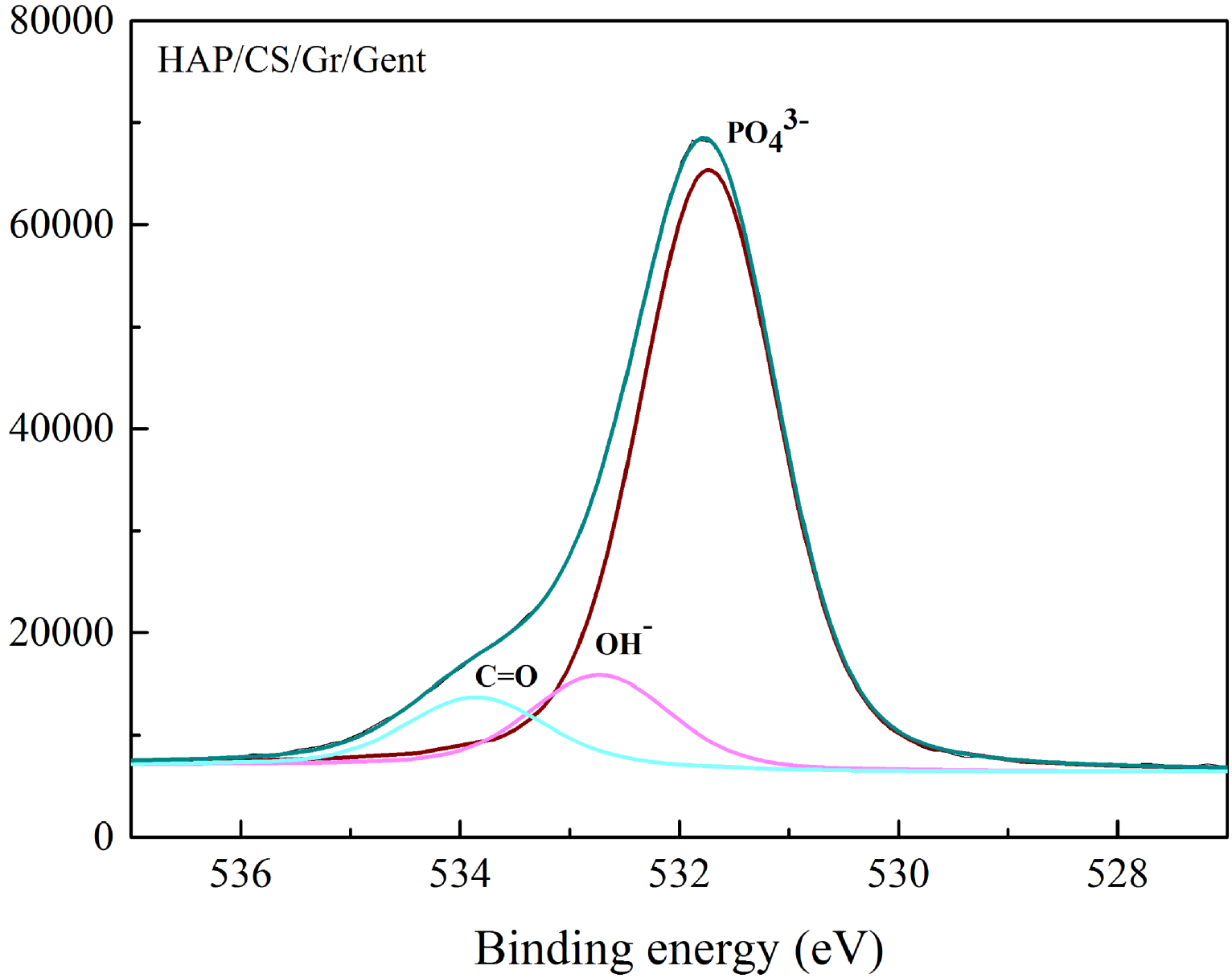

e)

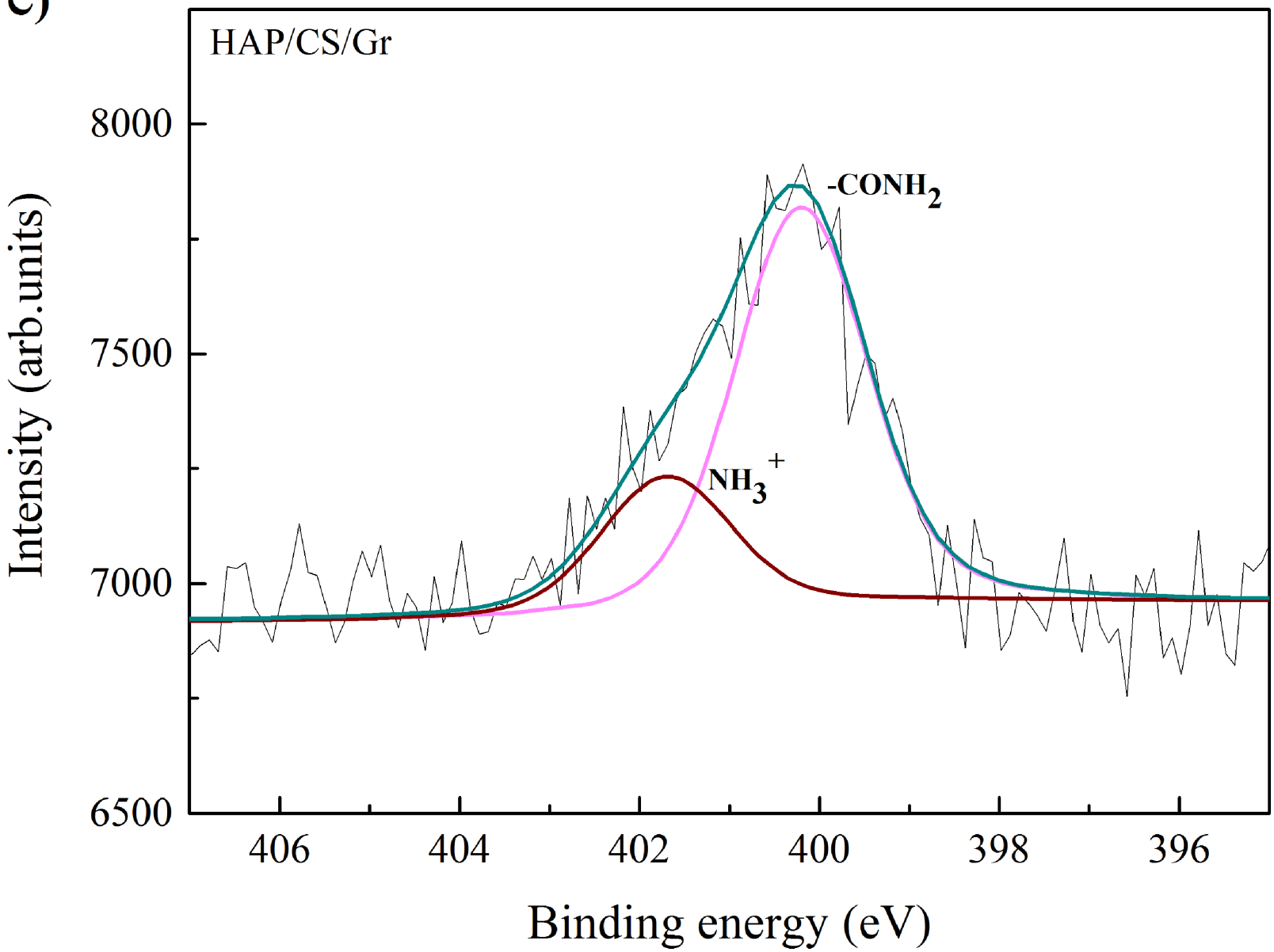

f)

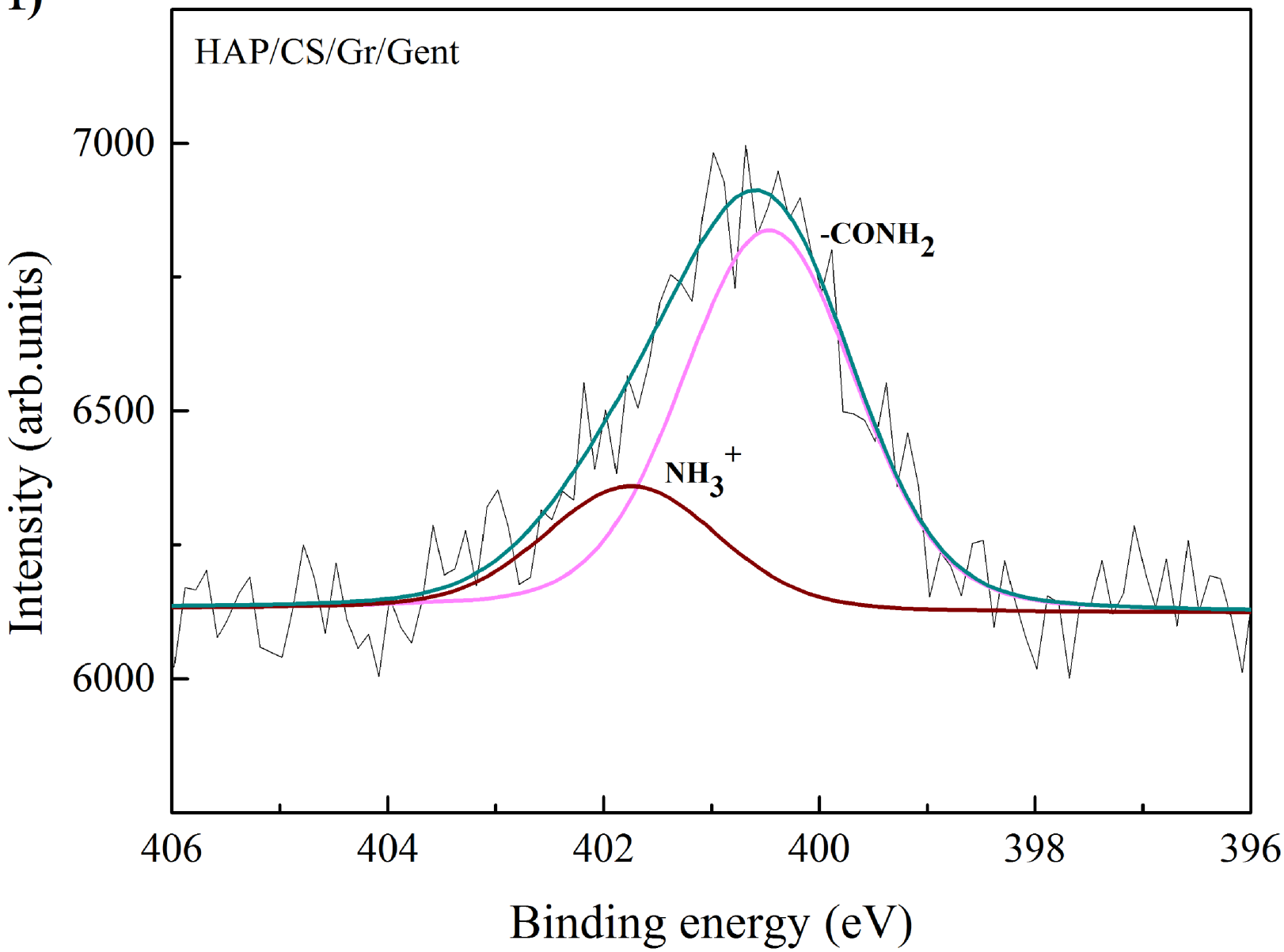

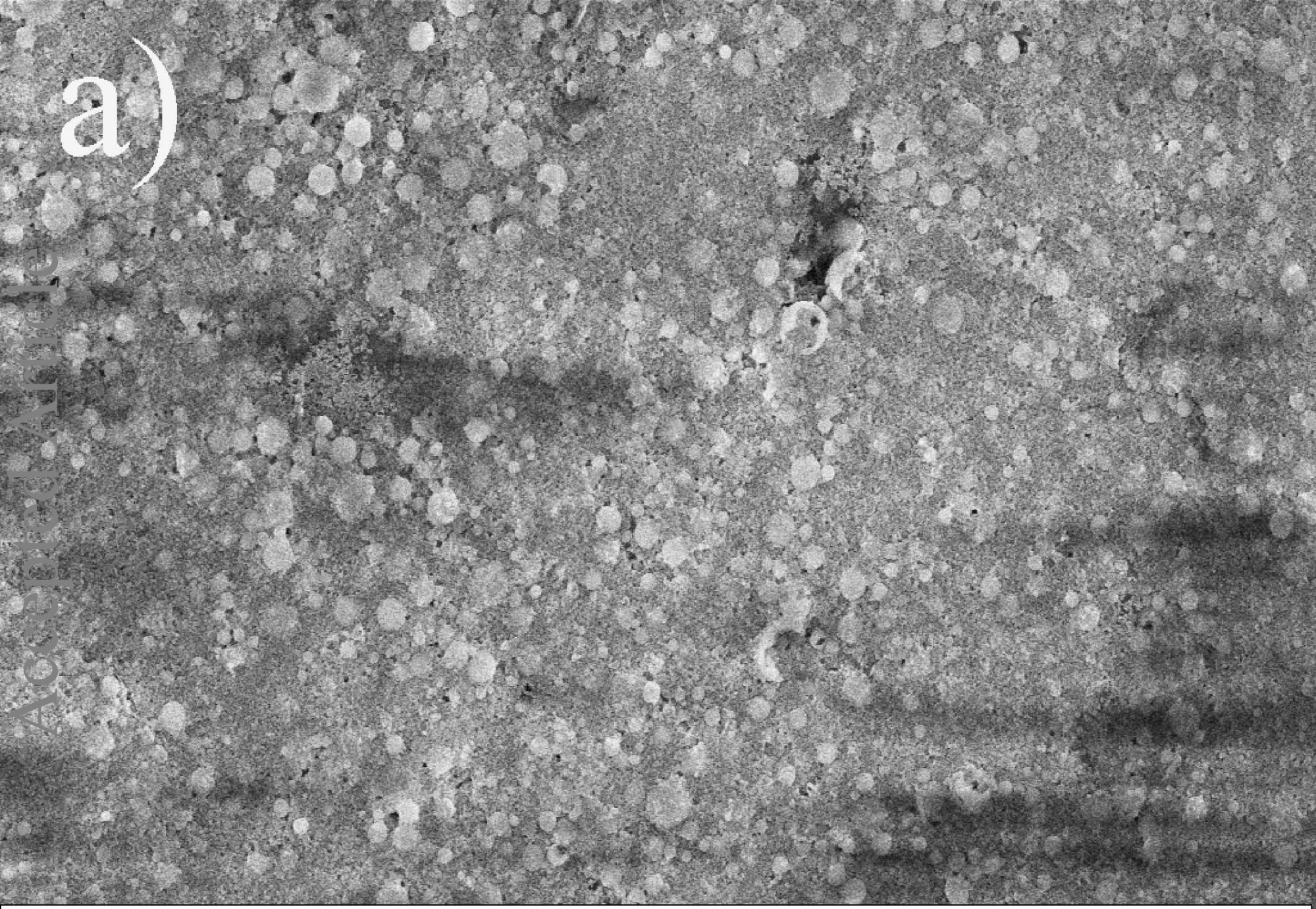
a)
1 µm
EHT = 10.00 kV
Mag = 10.00 K X
Signal A = InLens
WD = 7.8 mm
Contrast = 33.5 %
Date :19 Jun 2017
Kyung Hee
University

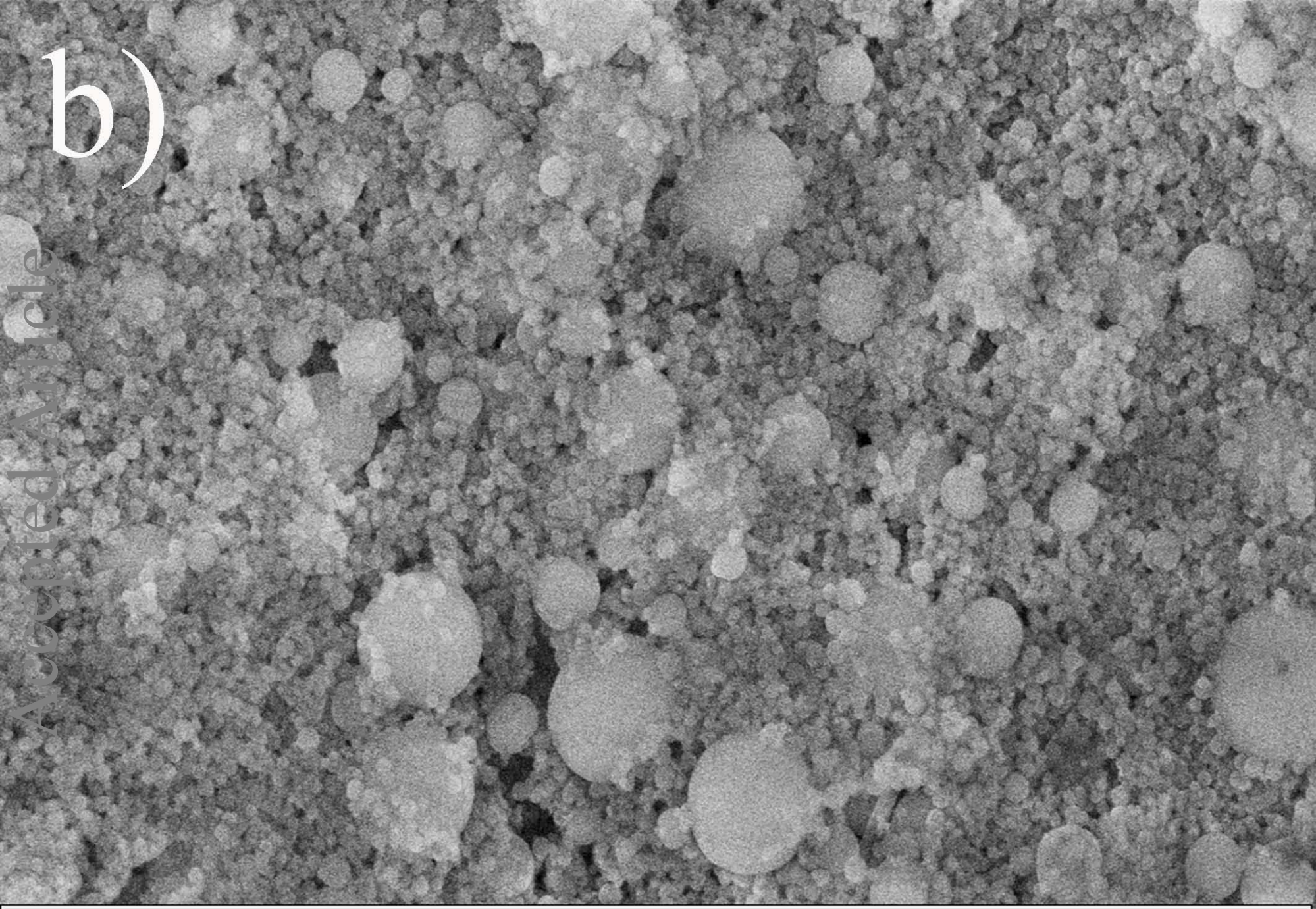

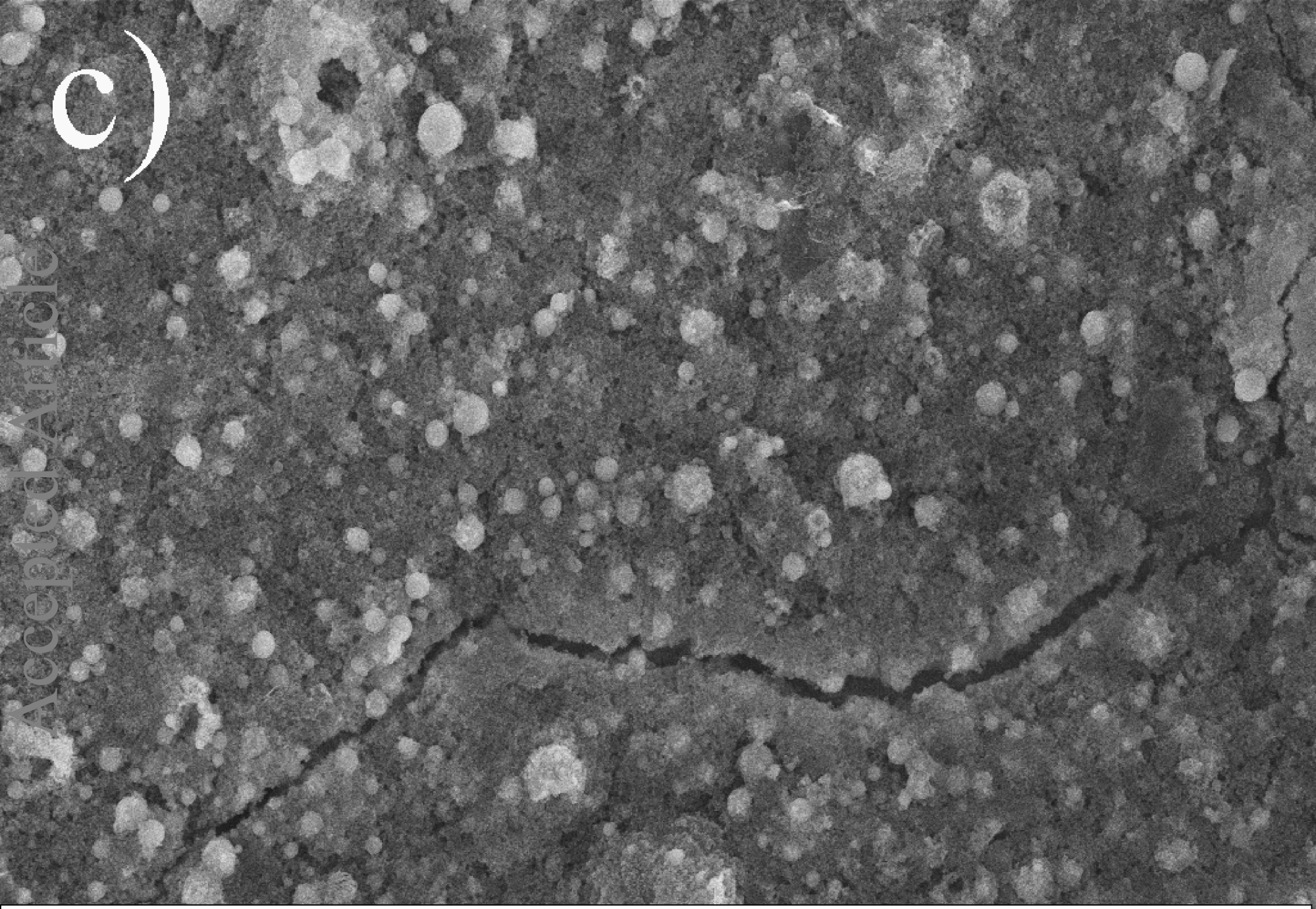

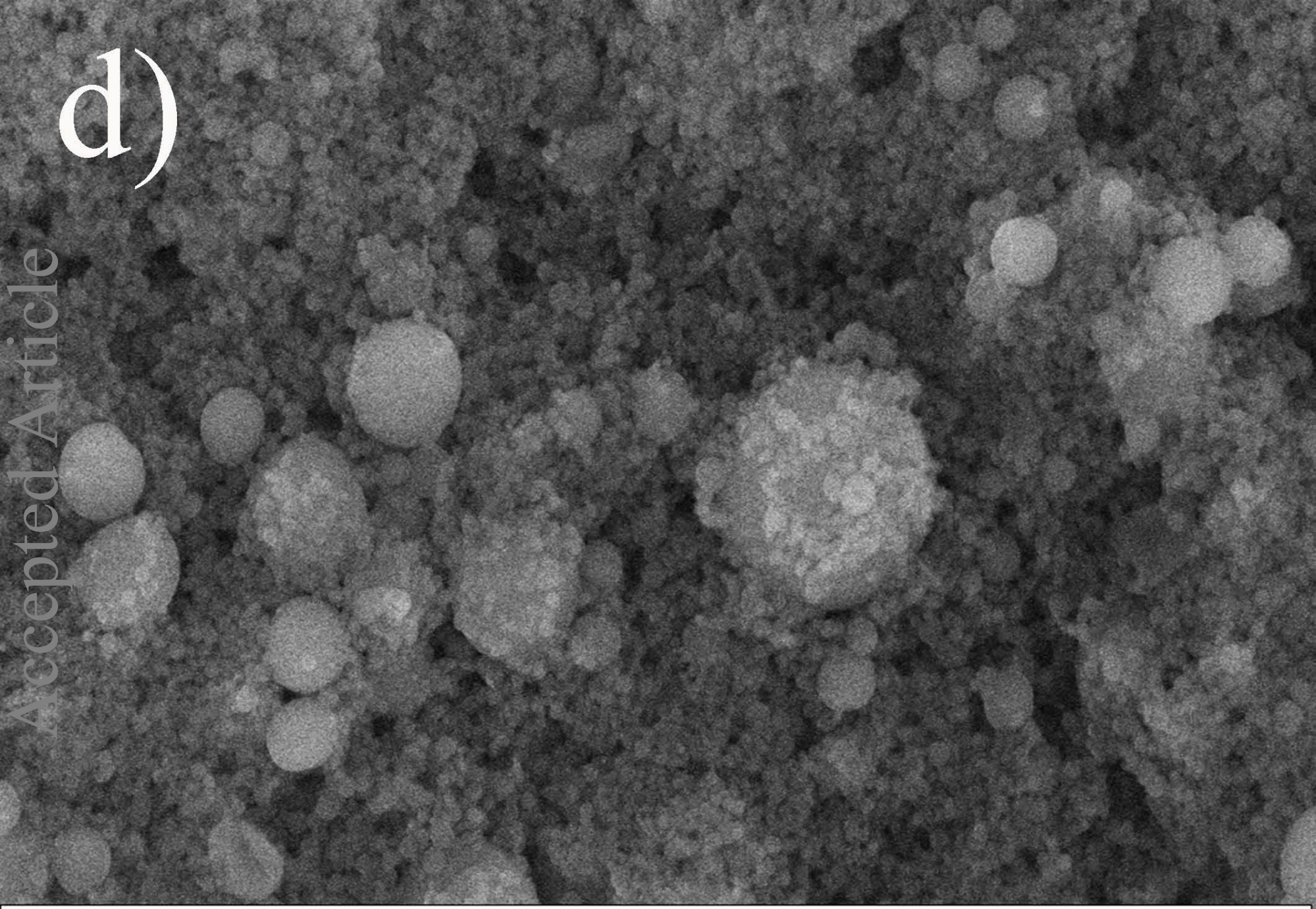

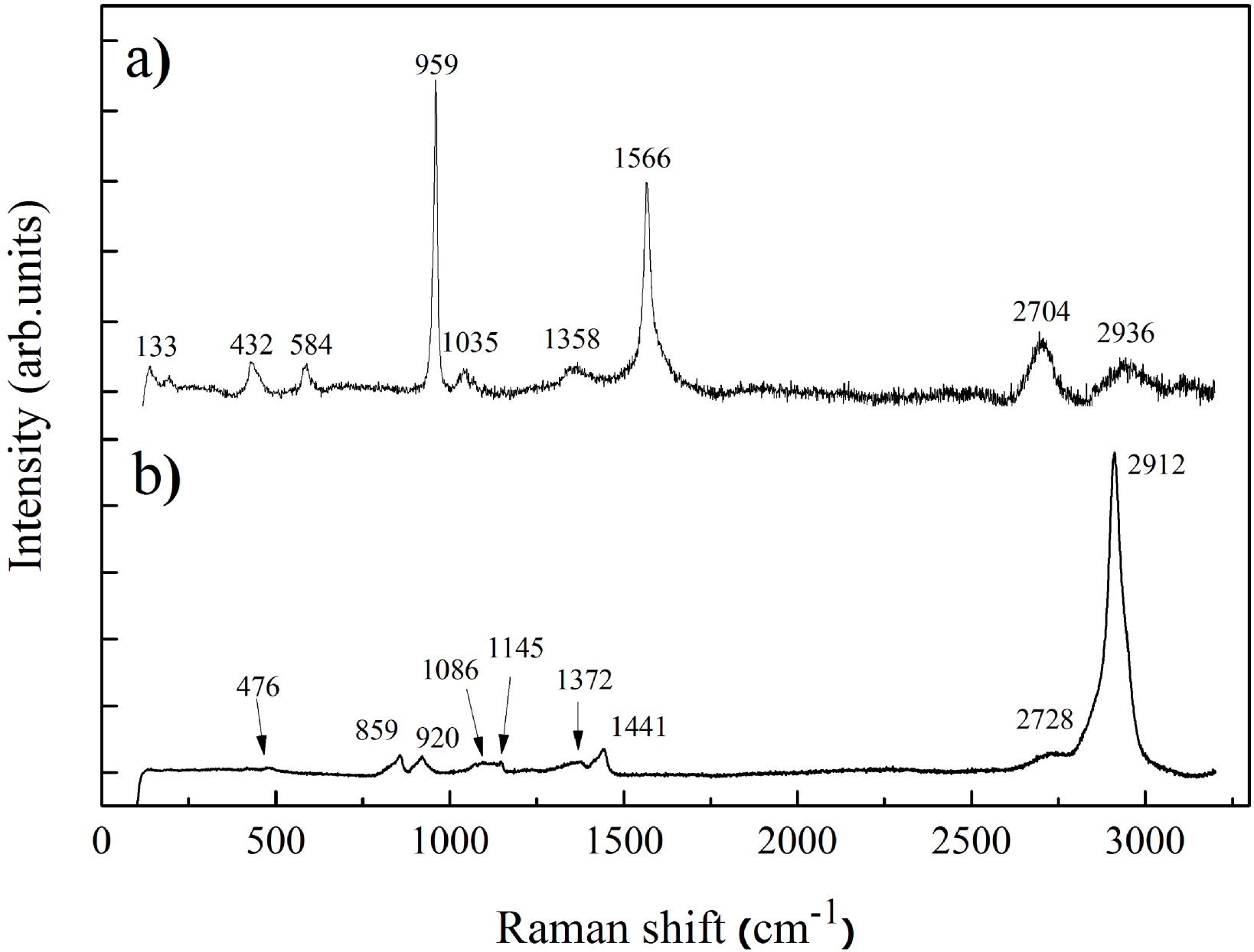

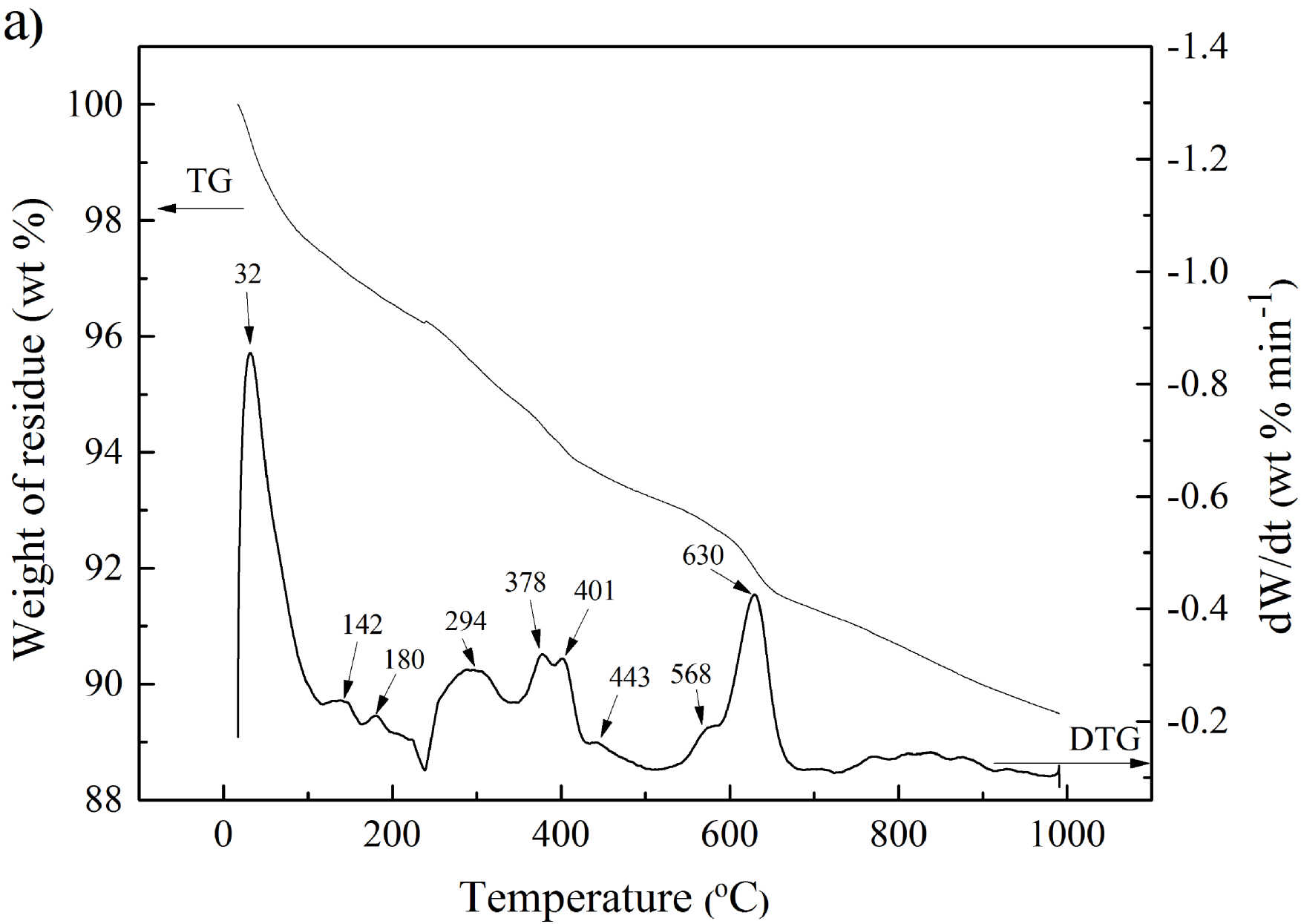

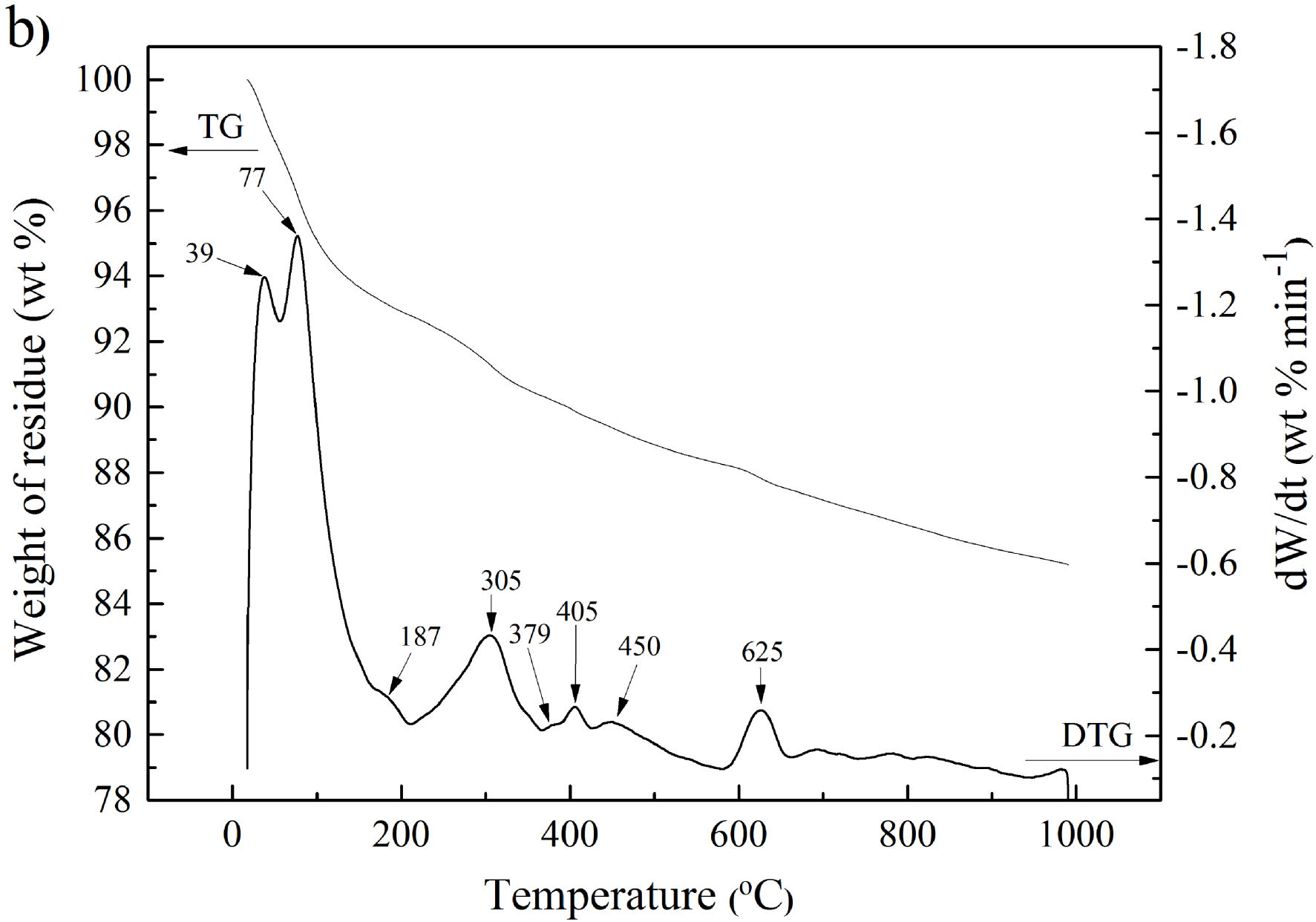

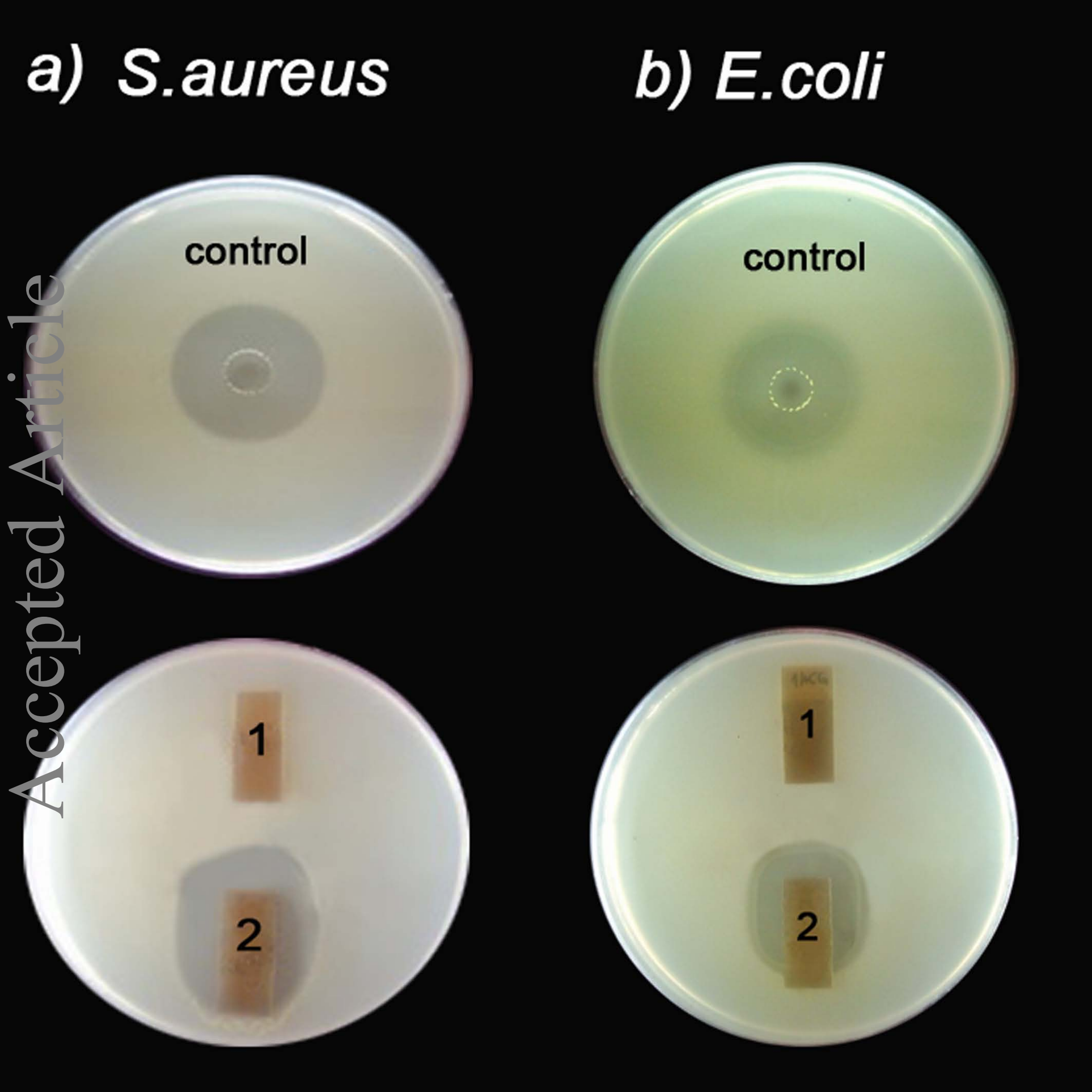

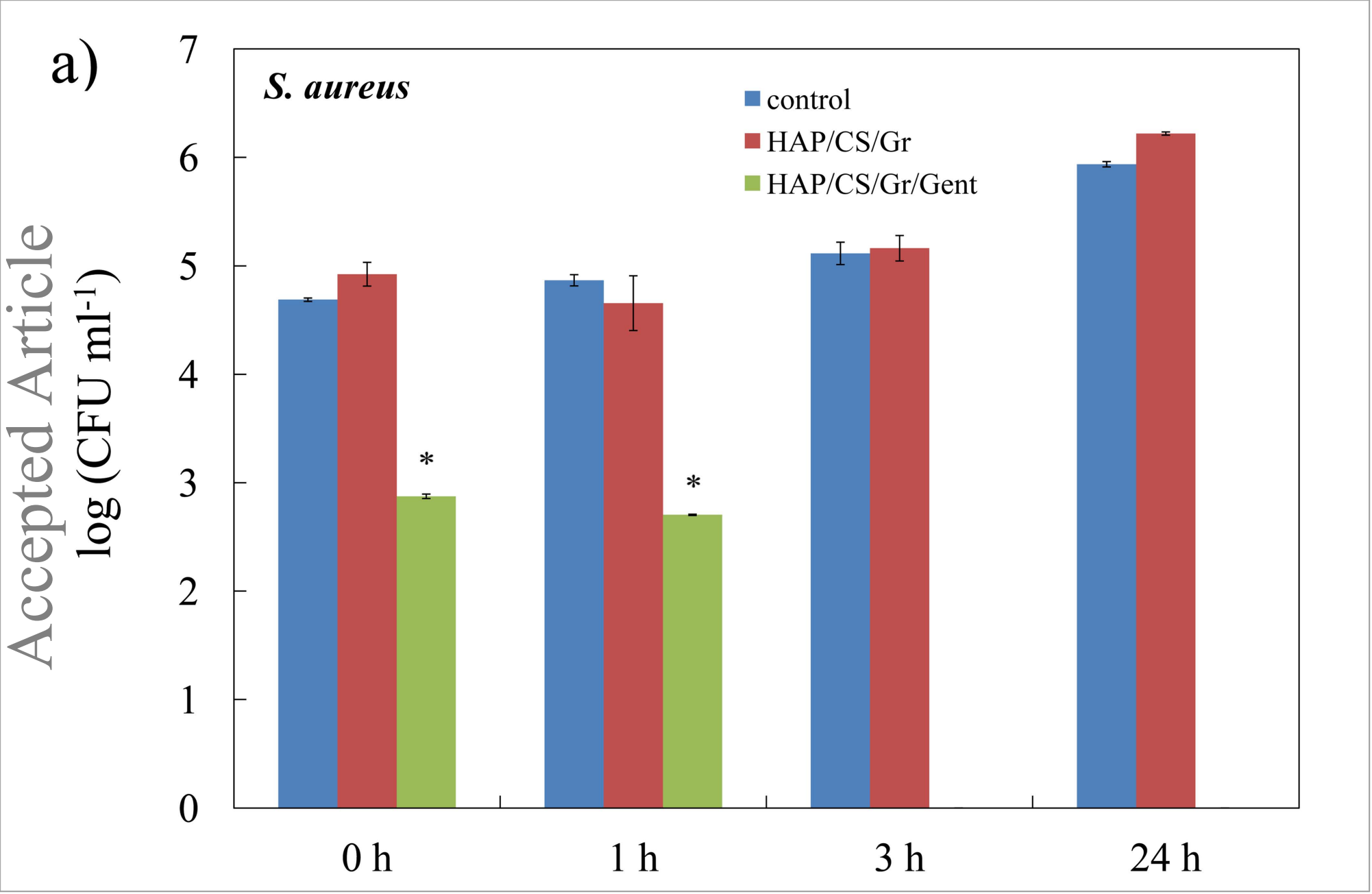
a)
S. aureus
control
HAP/CS/Gr
HAP/CS/Gr/Gent
Accepted Article
log (CFU ml-1)
0
1
2
3
4
5
6
7
*
*
0 h
1 h
3 h
24 h